Original Article

MOLECULAR METABOLISM

Nicotinamide riboside kinase 1 protects against diet and age-induced pancreatic β-cell failure

Angelique Cercillieux [1,2], Joanna Ratajczak [1,2], Magali Joffraud [1], José Luis Sanchez-Garcia [1], Guillaume Jacot [1], Alix Zollinger [1], Sylviane Métairon [3], Judith Giroud-Gerbetant [1], Marie Rumpler [1], Eleonora Ciarlo [1], Miriam Valera-Alberni [1,2], Audrey Sambeat [1], Carles Canto [1,2,*]

ABSTRACT

Objective: Disturbances in NAD^+ metabolism have been described as a hallmark for multiple metabolic and age-related diseases, including type 2 diabetes. While alterations in pancreatic β-cell function are critical determinants of whole-body glucose homeostasis, the role of NAD^+ metabolism in the endocrine pancreas remains poorly explored. Here, we aimed to evaluate the role of nicotinamide riboside (NR) metabolism in maintaining NAD^+ levels and pancreatic β-cell function in pathophysiological conditions.

Methods: Whole body and pancreatic β-cell-specific NRK1 knockout (KO) mice were metabolically phenotyped in situations of high-fat feeding and aging. We also analyzed pancreatic β-cell function, β-cell mass and gene expression.

Results: We first demonstrate that NRK1, the essential enzyme for the utilization of NR, is abundantly expressed in pancreatic β-cells. While NR treatment did not alter glucose-stimulated insulin secretion in pancreatic islets from young healthy mice, NRK1 knockout mice displayed glucose intolerance and compromised β-cells response to a glucose challenge upon high-fat feeding or aging. Interestingly, β cell dysfunction stemmed from the functional failure of other organs, such as liver and kidney, and the associated changes in circulating peptides and hormones, as mice lacking NRK1 exclusively in β-cells did not show altered glucose homeostasis.

Conclusions: This work unveils a new physiological role for NR metabolism in the maintenance of glucose tolerance and pancreatic β-cell function in high-fat feeding or aging conditions.

Keywords NAD^+; Nicotinamide riboside; Nicotinamide riboside kinase 1 (NRK1); Metabolic disease

1. INTRODUCTION

In the last decades, industrialized societies have seen a sharp increase in the prevalence of multiple interrelated metabolic complications, most notably insulin resistance and type 2 diabetes mellitus (T2DM). These disorders are tightly linked to a steady increase in the indexes of obesity and ageing. As such, the majority of patients with insulin resistance and T2DM are overweight and up to 80% are obese [1]. Along the same lines, around one third of elderly adults in western countries have abnormal glucose metabolism [2]. The etiology of insulin resistance and its transition onto overt T2DM involve a complex interplay of genetic and environmental factors, such as an inactive lifestyle [3]. Insulin resistance, generally described as an impairment in insulin action, markedly manifests as a reduction of insulin-stimulated glucose uptake in peripheral tissues. Early insulin resistant states, however, are not necessarily hyperglycemic, as pancreatic β-cells compensate for impaired insulin action by hypersecreting insulin. If left untreated, a chronic requirement for β-cell compensation can lead to β cell failure. At that point, pancreatic β-cells fail to secrete sufficient insulin to meet the metabolic demand, hence entering into T2DM.

Recently, strategies aimed to sustain cellular NAD^+ availability have shown significant success in pre-clinical models of insulin resistance. For example, the dietary supplementation with NAD^+ precursors, nicotinamide riboside (NR) or nicotinamide mononucleotide (NMN), prevented and/or alleviated glucose intolerance in insulin resistant models [4–7]. In addition, NMN has been shown to restore glucosestimulated insulin secretion (GSIS) in murine and human β-cells when challenged by hyperglycemia, hyperlipidemia or inflammatory cytokines [8,9]. Conversely, compromising NAD^+ levels in the pancreatic islets through genetic or pharmacological interventions was enough to cause defects in GSIS *in vivo* and *in vitro* [10]. The critical role of NAD^+ in situations of metabolic disease is not only linked to its role in hydride transfer reactions, but also as a degradation substrate for different families of enzymes, including sirtuins, ADP-ribosyltransferase enzymes (ARTDs, also known as PARPs) and NADases, such as CD38, CD157 and SARM1 [11,12]. These enzymes play critical roles in metabolic and transcriptional regulation, as well as DNA repair among others [11,12]. Some of the potential benefits of NAD^+ precursors have been linked to preserving the activity of sirtuins, most notably SIRT1. Accordingly, gain-of-function mouse models for

[1]Nestlé Institute of Health Sciences, Nestlé Research Ltd., Lausanne 1015, Switzerland [2]School of Life Sciences, Ecole Polytechnique Fédérale de Lausanne (EPFL), Lausanne 1015, Switzerland [3]Nestlé Institute of Food Safety and Analytical Sciences, Nestlé Research Ltd., Lausanne 1015, Switzerland

*Corresponding author. School of Life Sciences, EPFL - SV - LSBG, Station 19, 1015 Lausanne, Switzerland. E-mail: carles.canto@epfl.ch (C. Canto).

Received July 20, 2022 • Revision received September 10, 2022 • Accepted September 16, 2022 • Available online 20 September 2022

https://doi.org/10.1016/j.molmet.2022.101605

SIRT1 have consistently reported protection against diet and age-related insulin resistance [13–16]. Also, the overexpression of SIRT1 in pancreatic β-cells was enough to improve GSIS in mice [17]. Conversely, GSIS was impaired in islets where the SIRT1 gene had been deleted [18–20]. Several protective actions of SIRT1 on β-cell function have been proposed. For example, SIRT1 can act as a transcriptional repressor for the *Ucp2* gene, favoring the coupling between nutrient sensing and ATP synthesis [19]. Also, SIRT1 can suppress pro-inflammatory NF-κB signaling [21], while favoring the expression of transcription factors involved in the regulation of insulin content and β-cell maturation, such as NeuroD and MafA [22]. Therefore, these observations suggest that the dietary supplementation with NAD^+ precursors could provide health benefits in relation to glucose metabolism and pancreatic β-cell function.

NR and NMN are the NAD^+ precursors that have gained most attention during the last years. In contrast to the classic NAD^+ precursor nicotinic acid (NA), NR or NMN do not activate the G-coupled protein receptor GPR109A [4], responsible for most of NA undesirable side-effects, such as flushing [23]. The preclinical results obtained with NMN and NR are remarkably similar, which could be explained by the fact that NMN requires dephosphorylation to NR in order to enter the cell [24,25]. Once NR enters the cell, its transformation to NAD^+ is initiated by its phosphorylation, back to NMN, via the nicotinamide riboside kinase (NRK) enzymes [25,26] (Figure 1A). While most tissues express NRK1, NRK2 can also be found in skeletal muscle and, to a lesser degree, heart [25,27]. Interestingly, the ability of cells to use different molecules as NAD^+ precursors, including NA, nicotinamide (NAM) and NR, is evolutionarily conserved from yeast to humans [26]. This suggests that their roles might not be totally redundant for the physiological maintenance of cellular NAD^+ levels. This point is particularly critical when reasoning which NAD^+ precursor could be most suited for clinical success.

Here, we aimed to test the physiological role of the NR metabolism in healthy mice and in conditions of insulin resistance, such as high-fat feeding or aging. Our results first illustrate that NRK1 is abundantly expressed in pancreatic islets. The deletion of NRK1 did not have any major effect on baseline NAD^+ levels or glucose tolerance. However, NRK1 deletion exacerbated glucose intolerance in high-fat diet (HFD) fed mice. This glucose intolerance occurred in parallel to compromised GSIS by pancreatic β-cells. Interestingly, pancreatic β-cell specific NRK1 deficiency in mice did not recapitulate these phenotypes, suggesting that the defective pancreatic function stems from a systemic, rather than cell autonomous defect. Altogether, our results characterize how whole body NR metabolism is required to sustain pancreatic β-cell function in insulin resistant conditions.

2. MATERIALS AND METHODS

2.1. Animal models and housing

NRK1 whole body KO (NRK1 KO) mice have been described previously [25]. NRK1 β cell-specific KO (NRK1 BKO) mice were generated by crossing $NRK1^{LoxP/LoxP}$ mice [25,28] with mice expressing the Cre recombinase under the insulin 1 (*Ins1*) promoter (Ins1-Cre mice; obtained from the Jackson laboratory) [29]. Briefly, mice homozygous for the floxed *Nmrk1* gene were crossed with mice expressing in heterozygosity the Cre recombinase under the *Ins1* promoter. The Cre positive heterozygote pups were then subsequently crossed with *Nmrk1* floxed mice. The resulting homozygous *Nmrk1* floxed mice expressing the Cre recombinase (in heterozygosity) were then crossed with *Nmrk1* floxed mice. All mice used in the NRK1 BKO studies were generated through this strategy. In all experiments, NRK1 KO mice were compared to WT littermates, both being on pure C57BL/6NTac background. NRK1 floxed ($NRK1^{LoxP/LoxP}$) mice were used as control for NRK1 BKO littermates, all being on a mixed C57Bl/6NTac x C57BL/6J background.

All mice were maintained at a standard temperature of 22 °C and in a humidity-controlled environment with a 12:12h light–dark cycle. Mice were housed with appropriate nesting materials with ad libitum access to water and food (Safe® 150 diet). For the high-fat diet experiments, mice were exposed to a commercial high-fat diet (HFD, D12492 from Research Diets Inc.) or its control low-fat diet (D12450J, from Research Diets Inc.) at the age of 8 weeks. Male mice were used for the high-fat and aging studies, as female B6 mice are strongly protected against the development of insulin resistance and diabetes [5,30–33]. Male and female mice were used indistinguishably for all other purposes, including the validation of the different mouse lines and pancreatic islet studies in mice under normal housing conditions. All animal experiments were conducted according to Swiss and EU ethical guidelines and approved by the local animal experimentation committee (Service de la Consummation et des Affaires Veterinaries (SCAV) of the Canton de Vaud) under licenses VD 2770 and VD2770.1.

2.2. Animal phenotyping

For the HFD studies, all mice were ∼6 months of age by the time of sacrifice (24 weeks old). Specifically, mice were placed on a HFD (or the control low-fat diet) at 8 weeks of age. After 8 weeks on their respective diets (at 16 weeks of age), the following tests were performed prior to sacrifice (24 weeks old): indirect calorimetry (16 weeks-old), glucose tolerance tests (18 weeks old), insulin tolerance tests (20 weeks-old), treadmill and grip tests (22 weeks old) and non-invasive blood pressure assessment (23 weeks old). For the aging studies, young mice were ∼3 months of age (12 weeks old), while aged mice were ∼24 months of age (100–110 weeks old).

Oxygen consumption (VO_2), respiratory exchange ratio (RER), food intake and activity levels were monitored by indirect calorimetry using the comprehensive laboratory animal monitoring system (CLAMS, Columbus Instruments). Grip tests, treadmill tests and non-invasive blood pressure analyses were performed as previously described [4]. Glucose tolerance tests were performed after overnight fasting by measuring glycemia after an intraperitoneal injection of 2 g/kg glucose (Sigma G5146). Insulin tolerance tests were performed after a 6 h-fasting period, followed by the injection of 1.0 U/kg insulin (NovoRapid 058610). For fasting/refeeding experiments, glycemia and plasma insulin were evaluated after 24-hof fasting (Fasted). Mice were then fed, with access to food for 2 h before collecting blood for glycemia and insulin measurements. For experiments measuring active GLP-1, the refeeding time was 45 min. Insulinemia was measured in plasma samples using an ELISA kit (Sigma EZRMI-13K). At the end of the phenotyping, animals were euthanized via isoflurane inhalation after a 12-hour fast, in order to stabilize systemic parameters. Blood samples were collected in EDTA-coated tubes to retrieve plasma (centrifugation at 2000×*g*, 15 min, 4 °C). Tissues were collected upon sacrifice and flash-frozen in liquid nitrogen or fixed for histology.

2.3. Primary islet isolation and culture

Unless otherwise stated, primary islets were isolated from 12 to 20 week old mouse pancreas perfused with collagenase, as previously described [34]. Briefly, mice were euthanized with CO_2 followed by cervical dislocation. A ventral incision was then made to expose the upper abdomen of the mouse. Next, the ampulla of vater was clamped in order to block the bile duct to the duodenum. Then, 2 ml of collagenase V (Ref. C9263, from Sigma–Aldrich), diluted at

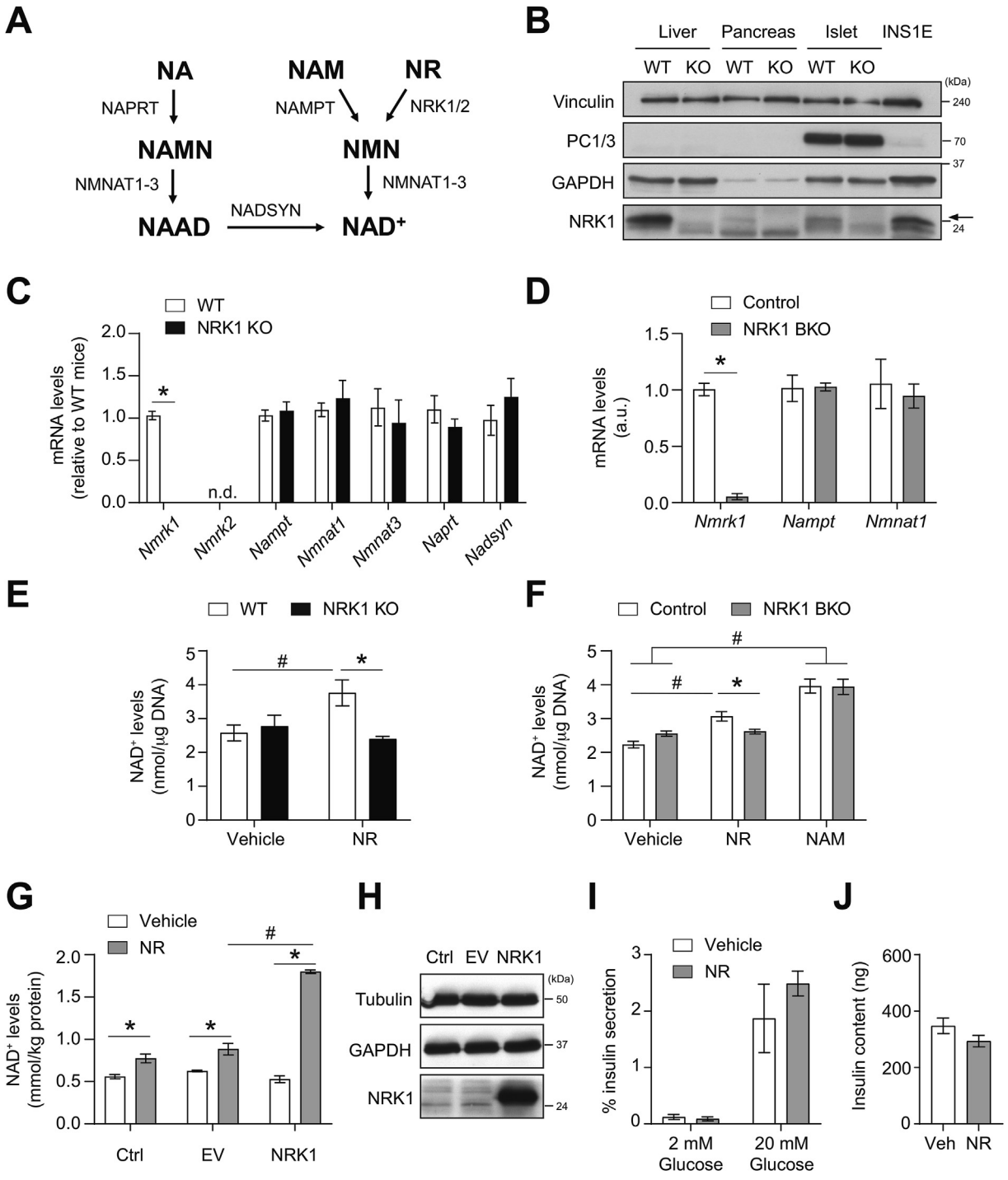

Figure 1: NR acts as a NAD$^+$ precursor in pancreatic β-cells. (A) NAD$^+$ biosynthesis paths used by nicotinic acid (NA), nicotinamide (NAM) and nicotinamide riboside (NR). In the figure, NAMN: NA mononucleotide; NAAD: NA adenine dinucleotide; NMN: NAM mononucleotide; NAPRT: NA phosphoribosyltransfersase; NMNAT: NMN adenylyltransferase; NADSYN: NAD synthase; NAMPT: Nicotinamide phosphoribosyltransferase; NRK: NR kinase. **(B)** Tissue homogenates from livers, pancreas and islets from ~-20 week old wild type (WT) and NRK1 KO (KO) mice were used for western blotting, together with protein homogenates from INS-1E cells. A representative image is shown. **(C)** Total RNA was extracted from WT and NRK1 KO islets and the expression of different NAD$^+$ metabolism enzymes was evaluated by real-time quantitative PCR. **(D)** Gene expression of NAD$^+$ metabolic enzymes in islets from control (*Nmrk1* floxed mice; white bars) and β-cell specific NRK1 KO mice (NRK1 BKO; grey bars). **(E)** Pancreatic islets from WT and NRK1 KO mice were collected and incubated with PBS (as vehicle) or NR (0.5 mM) for 2 h. Then acidic extracts were obtained to measure NAD$^+$ levels. **(F)** NAD$^+$ levels in pancreatic islets from either control or NRK1 BKO mice treated with PBS (as vehicle), NR (0.5 mM) or NAM (5 mM) for 2 h. **(G)** INS-1E cells were either left untreated (Ctrl) or transfected with empty vector (EV) or FLAG-NRK1 (NRK1) for 48 h prior to being treated with PBS (as vehicle) or NR (0.5 mM, 2 h). Then, acidic extracts were obtained to measure NAD$^+$ levels. **(H)** As in (G), but 48 h after transfection, protein homogenates were obtained to evaluate the efficacy of our transfection by western blot. **(I–J)** Islets from WT mice were collected and incubated with either PBS (as vehicle) or NR (0.5 mM, 2 h) prior the evaluation of glucosestimulated insulin secretion (GSIS). Insulin secreted to the media (I) and cellular insulin content (J) were then analyzed. All values are expressed as mean +/-SEM of n = 5 per genotype (C–D), or n = 8 WT mice and n = 4 NRK1 KO mice (E), or n = 4 per genotype (F), or n = 4 independent experiments (G–J). * indicates $p < 0.05$ vs. the respective WT or control group (C–F) or vs the vehicle group (E–G). # indicates $p < 0.05$ vs the vehicle or EV group within the same treatment (E–G).

2 mg/ml in Hank's Balanced Salt Solution (HBSS) containing 25 mM HEPES, were slowly injected into the common bile duct using a 5 ml syringe with a 30G 1/2-G needle. The perfused pancreas was then excised and placed on ice until it was moved to a 37 °C water bath for 5 min for collagenase digestion. Pancreas homogenates were washed 3 times with wash buffer (HBSS) with 0.5% (w/v) fatty acid free BSA). An average of 100 islets were handpicked from tissue homogenates using a dissection microscope and cultured in 10 mm dishes overnight at 37 °C in complete media (RPMI, 10% fetal bovine serum (FBS) and 1% Penicillin/Streptomycin) prior to performing any experiments. Male and female mice were used for islet studies, except for the high-fat diet and aging cohorts, where only males were used.

2.4. Cell culture

The INS-1E cell line was kindly provided by Prof. Claes B. Wollheim (University of Geneva). INS-1E cells, between passage 100—120, were used for all the experiments. Previous studies have demonstrated that the response of INS-1E to glucose challenges is preserved up to, at least, 142 passages [35]. All cells used in the study were verified as mycoplasma free using MycoProbe™ Detection kit (R&D cat. CUL001B). INS-1E cells were cultured in RPMI 1640 with L-Glutamine (ThermoFisher Scientific 21875034) supplemented with 10% FBS, 1% Penicillin/streptomycin, 10 mM HEPES, 1 mM Sodium pyruvate, and 50 μM β-mercaptoethanol. For studies on the overexpression of NRK1, 2 μg of plasmid DNA containing just the empty vector or encoding for a FLAG-tagged NRK1 protein [25] were transfected using JetPRIME® (Polyplus Transfection) according to manufacturer's instructions. All treatments were performed 48-hour post transfection. INS-1E cells were treated with 0.5 mM NR (Niagen, kindly provided by Chromadex Inc.), 5 mM Nicotinamide (Sigma N0636) or PBS (Vehicle) for 2 h prior to the evaluation of readouts.

2.5. –Glucosestimulated insulin secretion (GSIS)

Krebs-Henseleit (KH) buffers with low glucose (2 mM; KH-LG) or high glucose (20 mM; KH-HG) were prepared fresh, the day of the experiment. KH buffer was composed of 120 mM NaCl, 1.2 mM KH_2PO_4, 10 mM HEPES, 1.2 mM $MgSO_4$, 2.5 mM $CaCl_2$, 5 mM $NaHCO_3$, 4.8 mM KCl and 0.5% (w/v) fatty acid free BSA. PH was adjusted to 7.4 and buffer was filtered before being used. All buffers were brought to 37 °C prior to the experiment.

For primary islet studies, 20 islets were transferred to an Eppendorf tube (3—4 replicates per animal) and washed with KH buffer twice. Islets were then pre-incubated in 100 μl KH-LG for 1 h in a 37 °C incubator under constant gentle shaking. Supernatants were gently removed and replaced with fresh 100 μl of KH-LG buffer, and then cells were incubated for another hour in a 37 °C incubator shaking. The supernatants (basal insulin secretion) were collected in new Eppendorf tubes and kept on ice. Islets were next incubated in KH-HG for another 1 h in a 37 °C incubator under constant gentle shaking. Supernatants (GSIS) were then also collected in new Eppendorf tubes and placed on ice. Islets were resuspended in 100 μl of ice-cold acid EtOH (75 ml 100% EtOH, 1.5 ml 37% HCl, 23.5 ml H_2O) to measure insulin content. All samples were kept at −80 °C until the measurement of insulin.

For INS-1E cells, 3×10^5 cells were seeded on 24 well plate coated with poly-L-ornithine (1:10 dilution in PBS at 37 °C for 1 h) and cultured for 24—48 h before performing GSIS. On the day of the experiment, cells were washed 2× with KH buffer and pre-incubated with 1 ml of KH-LG for 1 h at 37 °C. Cells were then washed again with 1 ml of KH-LG and incubated again with KH-LG for 30 min at 37 °C. The supernatants (basal insulin secretion) were collected and transferred to deep-well 96 well plates. Excess buffer was carefully removed without disturbing the cells, which were then incubated in 1 ml of KH-HG for 30 min at 37 °C. The supernatants were then collected and transferred to a deep-well 96 well plate (GSIS) and excess buffer was carefully removed. Cells were then resuspended in 1 ml of ice-cold acid EtOH (75 ml 100% EtOH, 1.5 ml 37% HCl, 23.5 ml H_2O) and collected to evaluate insulin content. Both supernatant and cells were kept at −80 °C. until the measurement of insulin.

For all GSIS tests, insulin released in the media and insulin content in cells were quantified using Rodent Insulin Chemiluminescence ELISA (ALPCO 80-INSMR-CH01) according to manufacturer's instructions. Percent Insulin secretion was quantified by normalizing the amount of insulin secreted in the media to the insulin content in the islets.

2.6. NAD^+ measurements

NAD^+ was extracted from cells or tissues and quantified using an EnzyChrom NAD/NADH Assay Kit (BioAssay Systems) according to manufacturer's instructions. NAD^+ levels were corrected by tissue weight (mmol/kg), protein content of cells (mmol/kg protein) or DNA content of islets (mmol/ug DNA).

2.7. mRNA and protein analysis

Total RNA from tissues was extracted with TRIzol (Invitrogen) while total RNA of islets was extracted using RNAeasy Plus Micro kit (Qiagen 74034). RNA concentrations were measured with a Nanodrop 1000 (ThermoFisher Scientific). Total RNA (0.5-1 μg) was reverse transcribed (Superscript II, Life Technologies) with both oligo dT and random hexamer primers and RNase inhibitor (Roche) according to the manufacturer's protocol. Transcript levels were quantified using SYBR Green real time quantitative PCR (LightCycler, Roche). All primers used can be found in Supplementary Table S1. Gene expression levels were normalized to β2-microglobulin, and Hypoxanthine-guanine phosphoribosyltransferase (HPRT). Relative gene expression between genotypes was assessed using ΔΔCt method.

Protein extraction, quantification and western blotting were performed as described previously [25]. Briefly, proteins were extracted in lysis buffer (50 mM Tris-HCL at pH7.5, 150 mM NaCl, 5 mM EDTA, 1% NP40) containing protease and phosphatase inhibitors. Tissuelyzer (Qiagen) was used to homogenize the tissue and protein extracts were quantified using a BCA assay (Pierce). For western blotting, proteins were separated by SDS-PAGE and transferred onto nitrocellulose membranes. Membranes were blocked for 1 h with 5% BSA in TBS-Tween followed by an overnight incubation with primary antibody diluted in TBS-T with 0.5% BSA at 4 °C. Secondary antibodies were used at 1:20,000 dilution and incubated with membranes for 1 h at room temperature. Membranes were developed by enhanced chemiluminescence (Amersham). All primary antibodies and dilutions used are listed in Supplementary Table S2.

2.8. Hormones and peptides profiling

Circulating hormones and peptides levels were assessed from 100μl of plasma samples with Mouse Adipokine Array kit (ARY013, R&D systems), according to manufacturer's instructions. The intensity of the blot was analyzed using the Protein Array analyzer plugin for ImageJ. Active GLP-1 levels in plasma were measured using a U-plex mouse active GLP-1 assay (Ref: K15305K, from Meso Scale Diagnostics, LLC).

2.9. Respirometry on mouse tissues

Respiration of fresh mouse tissues were measured using high-resolution respirometry (Oroboros Oxygraph-2k, Oroboros Instruments) as described previously [36].

2.10. Histology analysis

Tissues obtained from mice were immediately fixed in 4% paraformaldehyde. Subsequent processing and staining were performed at the Histology Core Facility at EPFL as previously described [28]. Sirius Red and insulin/glucagon staining were performed using the fully automated Ventana Discovery XT (Roche Diagnostics). Images of entire tissues (at least n = 4 animals) were taken with Olympus VS120 and quantified using Qupath [37].

2.11. Transcriptomic analyses

For RNA extraction, islets were placed in a Matrix D tube (MP Biomedicals) with 600µl of lysis buffer from Agencourt RNAdvance Tissue Kit (Beckman Coulter). Samples were homogenized twice for 1 min at speed 6 on FastPrep-24™ (MP Biomedicals). Total RNA was extracted using the Agencourt RNAdvance Tissue Kit (Beckman Coulter) following the manufacturer's instruction. Total RNA was quantified using the Quant-iT™ RiboGreen™ RNA Assay Kit (Invitrogen) on a Spectramax M2 (Molecular Devices). Total RNA quality was assessed with Fragment Analyzer-96 using DNF-471-0500 Standard Sensitivity RNA Analysis Kit (Agilent Technologies). Next, 50 ng of total RNA ($8.9 < RQN < 10$) were used to generate the libraries using the QuantSeq 3′ mRNA-Seq Library Prep Kit FWD for Illumina (Lexogen) following 20 cycles of PCR amplification. Libraries were quantified using the Quant-iT™ Picogreen (Invitrogen) on a Spectramax M2 (Molecular Devices). Size pattern was assessed with Fragment Analyzer-96 using DNF-474-0500 High Sensitivity NGS Fragment Analysis Kit (Agilent Technologies). Libraries (average size of 242bp) were pooled at an equimolar ratio and clustered at a concentration of 9 pmol on a single read sequencing flow cell. 65 cycles of sequencing were performed on an Illumina HiSeq 2500 in rapid mode using a 50 cycles SBS kit (Illumina) according to manufacturer's instruction.

2.12. Statistical analysis

All statistical analysis were performed with Prism software (GraphPad). Sample size was determined based on previous experiments and published results. Differences between two groups were assessed using two-tailed *t*-tests. To compare the interaction between two variables, two-way ANOVA tests were performed. For comparing more than two groups to analyze variance, Turkey's or Dunnett's multiple comparison tests were used. All data are expressed as mean ± SEM. All p values < 0.05 were considered significant.

For statistical analyses in transcriptomic analyses, raw counts were obtained from mapping the sequences to the mouse reference genome using STAR v.2.5.3 and counting using htseq-count v.0.6.1. We first filtered the data by selecting only genes with a minimum of 5 reads in at least 8 samples. Specifically, threshold was set to 1.47 on the CPM values. We also discarded genes with no annotation. We kept 10,509 features with these filtering criteria. Trimmed Mean of M-value (TMM) normalization was used to account for composition bias between libraries. Differential expression analysis between different groups was performed using edgeR v3.20.9, which fits a negative binomial log-linear model to the normalized counts for each feature. Empirical Bayes methods were used to moderate the degree of overdispersion. We further extended the negative binomial model with quasi-likelihood method to account for gene-specific variability. Differential expression was assessed using quasi-likelihood F-tests. Resulting p-values were adjusted for multiple testing using Benjamini and Hochberg method (BH). For lowly expressed genes, we ran the same analysis above without the filtering step.

3. RESULTS

3.1. *NRK1 is expressed in pancreatic β-cells*

To evaluate the role of NR metabolism in glycemic control, we initially characterized the pancreatic expression of NRK1 in WT mice. The NRK1 protein was detectable in pancreas, albeit at much lower levels than in liver (Figure 1B). Interestingly, the rat insulinoma cell line INS-1E showed a remarkable NRK1 content (Figure 1B), which led us to think that, despite the relatively low levels of NRK1 in whole pancreas, NRK1 levels could be high in pancreatic islets. Supporting this, a clear enrichment in NRK1 was seen in isolated islets compared to the whole pancreas (Figure 1B). NRK1 was not detectable in tissues or islets from whole body NRK1 knock-out mice (NRK1 KO), further validating our mouse model (Figure 1B). To discern whether the expression of NRK1 in islets was attributable to pancreatic β-cells, we generated a pancreatic β-cell-specific NRK1 knock-out mice (NRK1 BKO) by crossing mice in which the *Nmrk1* gene was floxed (*Nmrk1*$^{fl/fl}$; referred to as control mice from here on) [28], with mice expressing the Cre recombinase under the *Ins1* promoter [29]. Islets from NRK1 BKO mice, as well as from NRK1 whole body KO mice (Figure 1C), showed close to undetectable mRNA or protein levels of NRK1 (Figure 1D and Figure S1A), suggesting that pancreatic β-cells are largely accountable for NRK1 expression in the mouse pancreas. As expected, *Nmrk1* gene expression was not affected in other tissues from the NRK1 BKO mice, such as liver, kidney or brain (Fig. S1B). Also, the mRNA levels of enzymes involved in NAD^+ synthesis from other paths were not altered in islets from either NRK1 KO or NRK1 BKO mice (Figure 1C and Figure 1D, respectively).

3.2. NR is a NAD^+ precursor in pancreatic islets

In most mammalian cells and tissues, NRK1 is the essential and rate limiting step for NR-mediated NAD^+ synthesis [25]. Therefore, the fact that NRK1 is expressed in pancreatic β-cells suggested that islets can use NR as a NAD^+ precursor. To validate this point, we isolated pancreatic islets from wild type (WT) or NRK1 KO mice and treated them with or without NR (0.5 mM, for 2 h). NAD^+ levels were comparable between WT and NRK1 KO islets when treated with the vehicle solution (PBS) (Figure 1E). In WT islets, NR treatment led to a ∼40% increase in NAD^+ levels (Figure 1E). In contrast, NR failed to increase NAD^+ levels in NRK1 deficient islets (Figure 1E). Similarly, NR did not increase the NAD^+ levels in islets from NRK1 BKO mice, but did so in islets from control floxed mice (Figure 1F). Importantly, an alternative NAD^+ precursor, nicotinamide (NAM, 5 mM), equally increased NAD^+ levels in islets from control and NRK1 BKO mice (Figure 1F), certifying that NRK1 deletion does not impair the ability of pancreatic islets to synthesize NAD^+ through other routes (Figure 1A).

We next aimed to test if the magnitude of the effect of NR on NAD^+ levels was determined by NRK1 expression in β-cells. For this, we evaluated the impact of NR on NAD^+ levels in INS-1E cells either non-transfected, transfected with an empty vector plasmid (EV), or transfected with plasmid encoding a FLAG-tagged form of NRK1. The results illustrate that the overexpression of NRK1 did not alter basal NAD^+ levels, yet largely magnified the effects of NR on intracellular NAD^+ levels (Figure 1G—H). Altogether, these observations indicate that NR can act as NAD^+ precursor in pancreatic β-cells and that NRK1 rate-limits the magnitude of the effect.

Finally, we evaluated whether NR treatment would lead to functional changes in pancreatic β-cells. For this, we first isolated pancreatic islets from WT mice and exposed them to NR for 2 h , which is enough to increase NAD^+ levels (Figure 1E). Then, we examined GSIS in the

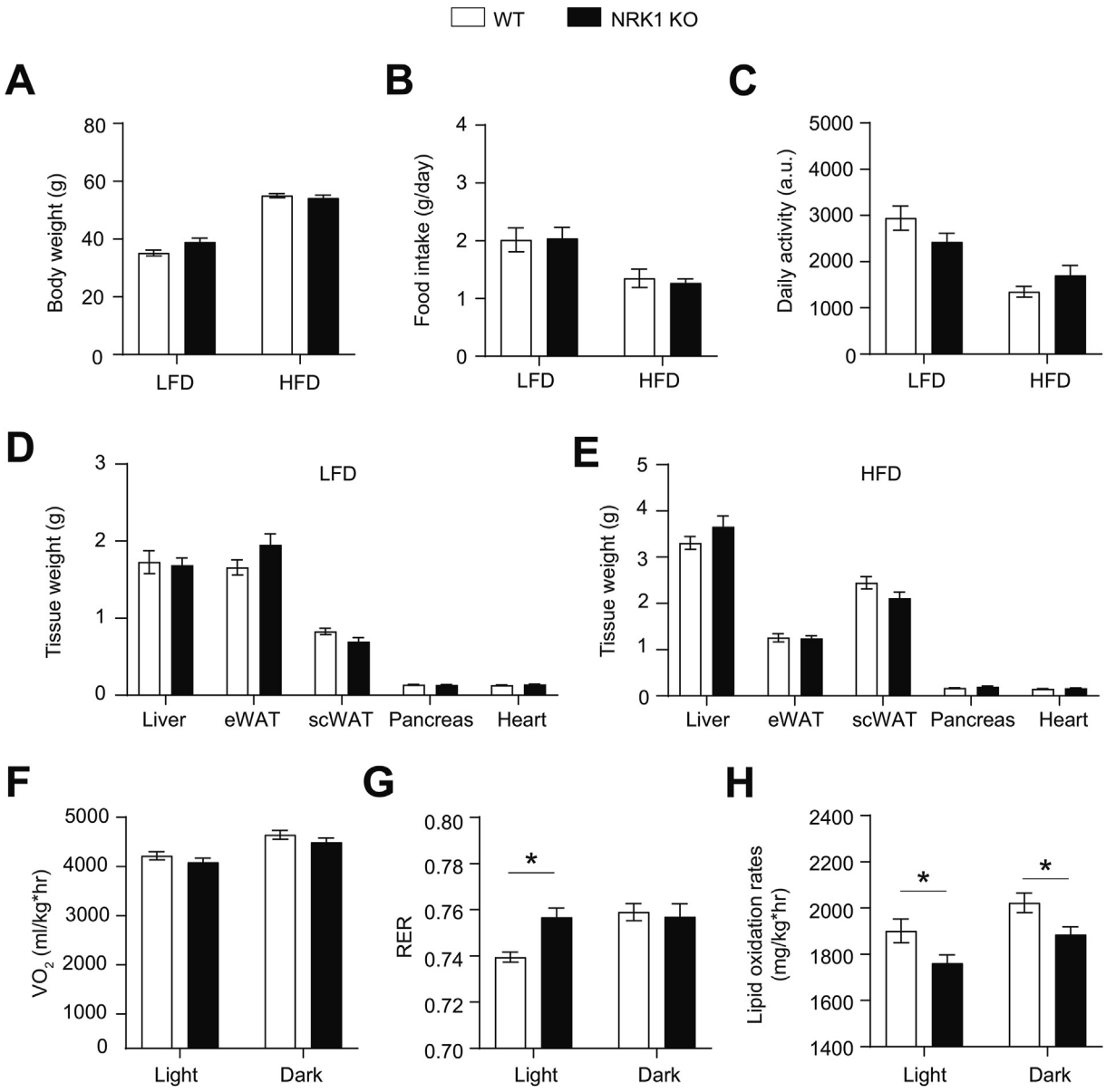

Figure 2: NRK1 KO mice display alterations in lipid oxidation rates upon high-fat feeding. Eight week old wild type (WT) and NRK1 KO mice were placed on either a low-fat diet (LFD) or a high-fat diet (HFD). **(A)** Body weight of WT and NRK1 KO mice 16 weeks after the initiation of the LFD or HFD treatments. **(B—C)** Food intake (B) and daily activity (C) were evaluated 8 weeks after the initiation of the regimes, using a comprehensive laboratory animal monitoring system (CLAMS, Columbus instruments). **(D—E)** Tissues weight from LFD (D) or HFD (E) fed animals were determined 16 weeks after the initiation of the diets. **(F—H)** WT and NRK1 KO mice submitted to a HFD were used for indirect calorimetry experiments using a CLAMS systems 8 weeks after the initiation of the dietary intervention. VO_2 values (F), respiratory exchange ratios (RER; VCO_2/VO_2) (G) and lipid oxidation rates (H) were then estimated. Through the figure, white bars represent WT mice, while black bars represent NRK1 KO mice. All values are expressed as mean +/− SEM of n = 10 mice for the WT group and n = 11 mice for the NRK1 KO group. * indicates $p < 0.05$ vs. the respective WT group.

media. GSIS was similar between vehicle and NR-treated islets (Figure 1I). Similarly, NR treatment did not alter insulin content in the islets (Figure 1J). Overall, these results suggest that acutely raising NAD^+ levels with NR does not influence GSIS in β-cells from young healthy mice.

3.3. NRK1 KO mice display pancreatic dysfunction upon high-fat feeding

To better understand the physiological impact of NR metabolism in pancreatic β-cell function and glucose metabolism, we placed 8 week-old WT and NRK1 KO mice either on a low-fat diet (LFD) or a high-fat diet (HFD) (Research Diets 12450J and 12492, respectively). High-fat feeding similarly increased body weight in both genotypes (Figure 2A). Also, no differences were observed in food intake (Figure 2B), daily activity (Figure 2C) or individual tissue weights (Figure 2D—E) between genotypes, either under LFD or HFD. WT and NRK1 KO mice performed equally in response to a treadmill challenge (Figure S2A). Also, blood systolic pressure values and heartbeat rates were similar among genotypes, except for a modest decrease in heartbeat rate in NRK1 KO mice when exposed to a HFD (Figure S2B-C). Next, we examined metabolic rates by indirect calorimetry. The results revealed that on LFD, O_2 consumption (VO_2), respiratory exchange ratios (RER) or lipid oxidation rates were comparable between genotypes (Figure S2D-F). On HFD, while O_2 consumption was similar (Figure 2F), RER values

were higher on NRK1 KO mice during the light phase (Figure 2G). When lipid oxidation rates were estimated from indirect calorimetry values, the results illustrated lower lipid oxidation rates in NRK1 KO mice through the day (Figure 2H).

The slight differences in substrate utilization in HFD-fed NRK1 KO mice went in parallel to alterations in glucose metabolism. Accordingly, while glucose tolerance was similar between WT and NRK1 KO mice fed a LFD (Figure S3A), HFD-fed NRK1 KO mice displayed exacerbated glucose intolerance compared to WT littermates (Figure 3A). When analyzing insulin secretion during the glucose tolerance test, the results reflected again no difference in GSIS in LFD-fed mice (Fig.S3B). However, insulin secretion was dramatically impaired in NRK1 KO mice fed a HFD (Figure 3B). This was not consequent to a higher insulin response, as NRK1 KO mice showed a slightly impaired insulin effects during insulin tolerance tests (Figure 3C). This led us to quest for possible alterations in the pancreatic islets of NRK1 KO mice under HFD. Histology analyses reveled that, while islets were similar in number between genotypes, they were larger in size in NRK1 KO mice (Figure 3D—F), leading to increased α-cell and β-cell mass (Figure 3G—H). To directly evaluate alterations in pancreatic islet function, we collected mouse islets from either LFD- or HFD-fed WT and NRK1 KO mice to evaluate insulin content and perform GSIS assays *ex vivo*. Insulin content and GSIS were similar in islets from WT and NRK1 KO mice when fed a LFD (Figure 3C and Figure S3D). However, GSIS was critically impaired in islets from HFD-fed NRK1 KO mice (Figure 3I), which also displayed lower insulin content (Figure 3J). Altogether, these results indicated that NRK1 deletion leads to a severe pancreatic β-cell dysfunction upon high-fat feeding. To further investigate the potential cause of β-cell dysfunction in NRK1 KO mice, we assessed the expression of genes important for β-cell maturation and glucose sensing in islets from WT and NRK1 KO mice under a HFD. The results revealed that islets from NRK1 KO mice exhibited decreased expression of glucokinase (*Gck*) and the MafA transcription factor (*MafA*) (Figure 3K), which are critical players in glucose sensing and β-cell specific gene expression, respectively. Notably, these changes were not observed in NRK1 KO mice when fed a LFD (Figure S3E).

3.4. Aged NRK1 KO mice display impaired pancreatic function

In addition to obesity, aging is another major risk factor for insulin resistance and T2DM. For this reason, we next evaluated the impact of aging on whole body metabolism and pancreatic function in NRK1 KO mice. At ∼24 months of age, WT and NRK1 KO mice had comparable body and tissue weight profiles (Figure 4A,B). Energy expenditure analyses through indirect calorimetry showed that, as observed in response to a HFD, aged NRK1 KO mice displayed similar VO_2 levels as WT littermates, yet they displayed higher RER values and lower lipid oxidation rates, especially in the dark phase, suggestive of impaired lipid oxidation capacity (Figure 4C—E). Aged NRK1 KO mice also displayed a clear tendency towards glucose intolerance upon an intraperitoneal glucose tolerance test (Figure 4F). This might be explained by the fact that circulating insulin levels in response to the glucose bolus were lower in NRK1 KO mice (Figure 4G). The alterations in glucose homeostasis and pancreatic function were also evident in response to a fasting challenge. After a 24 h fast, aged NRK1 KO mice displayed lower fasting glycemia (Figure 4H). This could not be explained by higher circulating insulin levels, as they were also lower (Figure 4I). In addition, insulin tolerance tests ruled out the possibility that NRK1 KO mice were more responsive to insulin (Figure 4J). When mice were refed for 2 h after the 24 h fast, circulating glucose levels increased to similar levels in WT and NRK1 KO mice (Figure 4H), yet circulating insulin levels remained significantly lower in NRK1 KO mice (Figure 4I). All these observations suggest that aged NRK1 KO mice exhibit impaired GSIS.

While the pancreas from aged WT and NRK1 KO mice had a similar weight (Figure 4B), histology analyses revealed a lower number and smaller size of islets in NRK1 KO mice (Figure 5A—C). Accordingly, pancreatic β-cell and α-cell mass were also reduced in NRK1 KO mice (Figure 5D—E), leading to a marked decrease of pancreatic insulin and glucagon content (Figure 5F—G). Surprisingly, when examining isolated islets, no major differences were observed in GSIS, insulin content per islet or in the expression of diverse mRNA makers of β-cell function and maturation (Figure 5H—J). In addition to reduced islet counts, the pancreas of NRK1 KO mice displayed larger fibrotic deposits, as evaluated by Sirius Red staining (Fig.5K-L). Collectively, these results suggest that both HFD and aging led to pancreatic dysfunction in NRK1 KO mice, albeit through different mechanisms. In the case of HFD, impaired GSIS was related to dysfunctional pancreatic β cells, while lower insulin release in aged mice might stem from reduced β-cell mass, but not intrinsic functional differences at the islet level.

3.5. Pancreatic dysfunction in NRK1 KO mice is not β-cell autonomous

We next interrogated whether deleting NRK1 exclusively in pancreatic β-cells would be enough to recapitulate the impaired GSIS observed in the whole body NRK1 KO mice upon HFD or aging. To test this hypothesis, we initially phenotyped the control and NRK1 BKO mice on either a LFD or a HFD. Body weight, food intake and daily activity were undistinguishable between genotypes, irrespectively of the diets (Figure S4A-C). While NRK1 KO on HFD showed changes in the outcomes of indirect calorimetry tests (Figure 2F—H), the deletion of NRK1 exclusively in pancreatic β-cells did not lead to differences in whole body VO_2, RER or lipid oxidation rates (Figure S4D-F). Furthermore, in contrast to the whole body NRK1 KO mice, the NRK1 BKO mice did not exhibit signs of altered glucose tolerance upon high-fat feeding (Figure S4G), and the insulin secretion profiles were comparable to those of control mice (Figure S4H). When analyzing pancreas parameters, we found no differences in pancreatic islet size, content, β-cell mass or α-cell mass (Figure S4I-L). Finally, gene expression analyses revealed no major changes in any of the genes examined (Supplementary Table S3). Therefore, the deletion of the *Nmrk1* gene specifically in β-cells did not lead to any major metabolic alteration, and NRK1 BKO mice did not recapitulate the deficiencies observed in whole-body NRK1 KO mice upon high-fat feeding.

In a very similar fashion, we failed to observe any critical metabolic alteration in aged NRK1 BKO mice compared to control littermates. Neither body weight, nor fasting glucose differed between genotypes (Figure S5A-B). In contrast to the aged NRK1 whole body KO mice, aged NRK1 BKO did not show altered circulating levels of insulin after a fasting/refeeding challenge (Figure S5C). Furthermore, NRK1 BKO did not show changes in glucose or insulin excursions after a glucose challenge (Figure S5D-E). Therefore, NRK1 BKO also failed to recapitulate the pancreatic defects observed in NRK1 whole body KO mice.

3.6. NRK1 deletion promotes systemic metabolic damage

Collectively, the work on NRK1 BKO mice highlighted how the defects in insulin secretion observed in NRK1 KO mice did not stem from the deletion of NRK1 in β-cells. This led us to hypothesize that the pancreatic failure in NRK1 KO mice was secondary to functional alterations in other tissues. As a first approach to evaluate this possibility we examined the impact of NRK1 deletion on NAD^+ levels in different tissues from young (3 month old) and old (24 month old) mice. NRK1

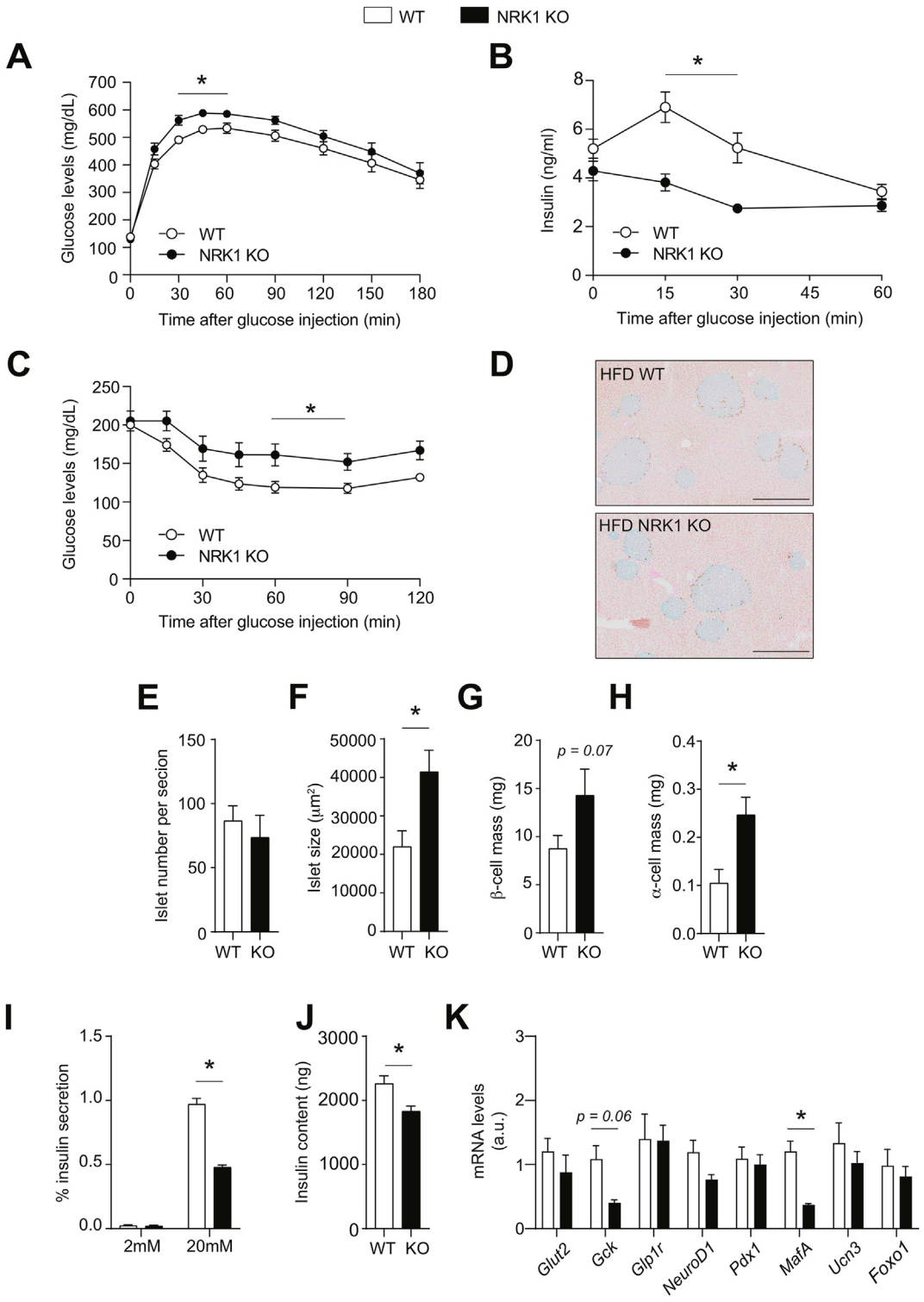

Figure 3: NRK1 KO mice under HFD exhibit pancreatic β-cell dysfunction. (A–B) intraperitoneal glucose tolerance tests (ipGTT) were performed on HFD-fed wild type (WT) and NRK1 KO mice 10 weeks after the initiation of the dietary regime. Glucose excursions (A) and circulating insulin levels (B) were then evaluated. **(C)** Intraperitoneal insulin tolerance tests (ipITT) were performed on HFD-fed WT and NRK1 KO mice 12 weeks after the initiation of the dietary regime. **(D–H)** Histological evaluation and quantifications for pancreatic islets characteristics in HFD-fed WT and NRK1 KO mice. The scale bar on (D) is set at 500 μm. **(I–J)** Pancreatic islets from WT and NRK1 KO mice submitted to a HFD for 16 weeks were used for *ex vivo* glucose-stimulated insulin secretion (GSIS) assays. In (I), % of insulin secretion in the media is shown, while (J) displays total insulin content in islets**. (K)** Total RNA was isolated from WT and NRK1 KO pancreatic islets, 16 weeks after the initiation of the diet, and multiple markers were analyzed by real time quantitative PCR. Through the figure, white bars represent WT mice, while black bars represent NRK1 KO mice. All values are expressed as mean +/− SEM of n = 10 WT mice and n = 11 for NRK1 KO mice (A–C). For histology image analysis, all values are expressed as mean +/−SEM of entire pancreas sections from n = 4 per mice genotype (E–H). For the work on isolated islets, values are expressed as mean +/− SEM of n = 5 mice per genotype (I–J) or n = 5 WT mice and n = 4 NRK1 KO mice (K). * indicates $p < 0.05$ vs. the respective WT group.

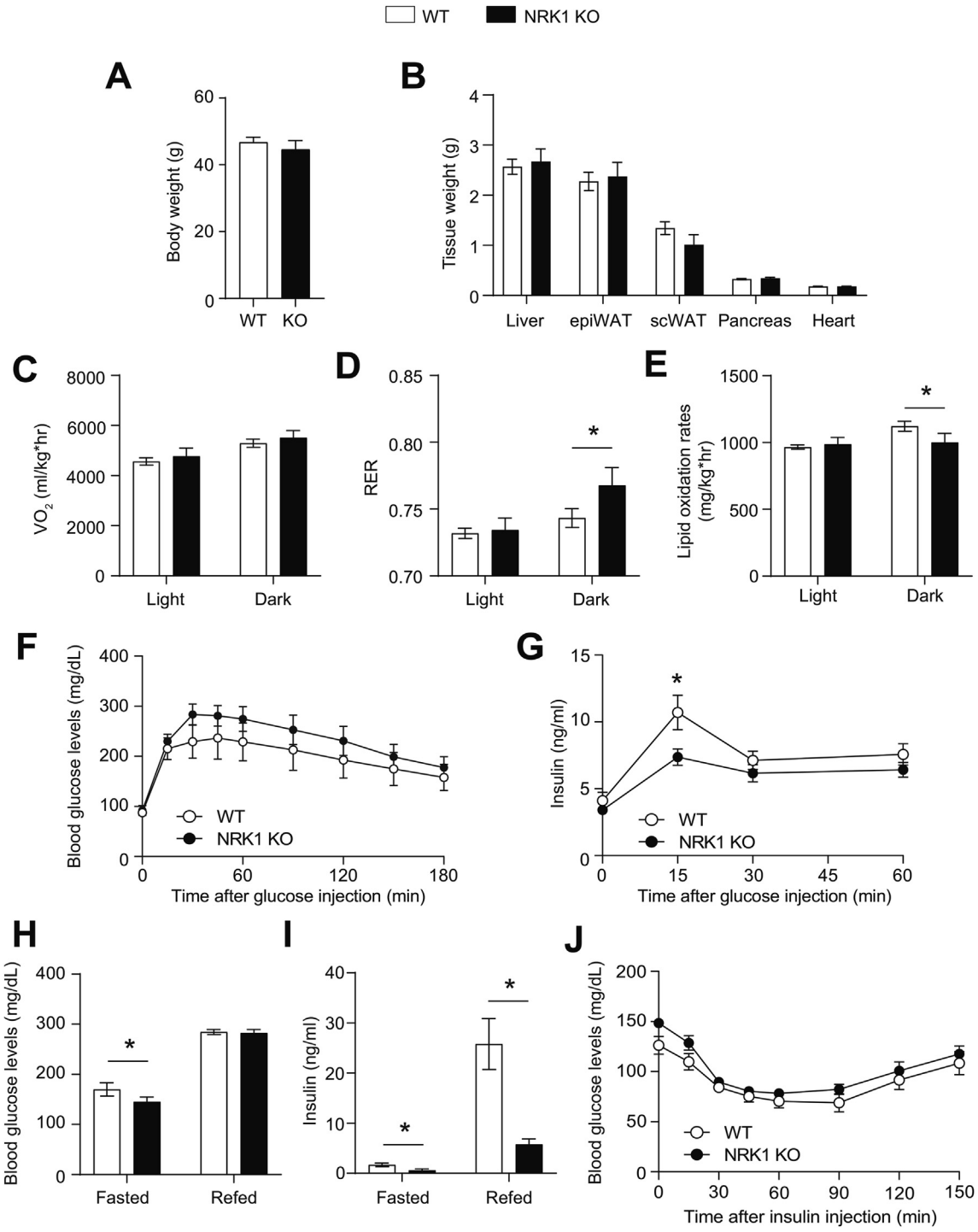

Figure 4: Metabolic abnormalities in aged NRK1 KO mice. (A—B) Body (A) and tissue (B) weights of wild type (WT) and NRK1 KO mice at 24 months of age. **(C—E)** WT and NRK1 mice, around 23 months of age were used for indirect calorimetry experiments using a CLAMS systems. VO_2 values (C), respiratory exchange ratios (RER; VCO_2/VO_2) (D) and lipid oxidation rates (E) were then estimated. **(F—G)** Intraperitoneal glucose tolerance tests were performed on ~23 month old WT and NRK1 KO mice. Glucose excursions (F) and circulating insulin levels (G) were then evaluated. **(H—I)** 22 month old WT and NRK1 mice were fasted for 24 h and the refed for 2 h. Blood glucose (H) and insulin (I) levels were analyzed in the fasted and refed state. **(J)** WT and NRK1 KO at 23—24 months of age were challenged with 1 U/kg of insulin after a 6 h fast. Then, blood glucose levels were evaluated for 2 h. Through the figure, white bars represent WT mice, while black bars represent NRK1 KO mice. All values are expressed as mean +/− SEM of n = 12 for WT mice and n = 11 for NRK1 KO mice. * indicates $p < 0.05$ vs. the respective WT group.

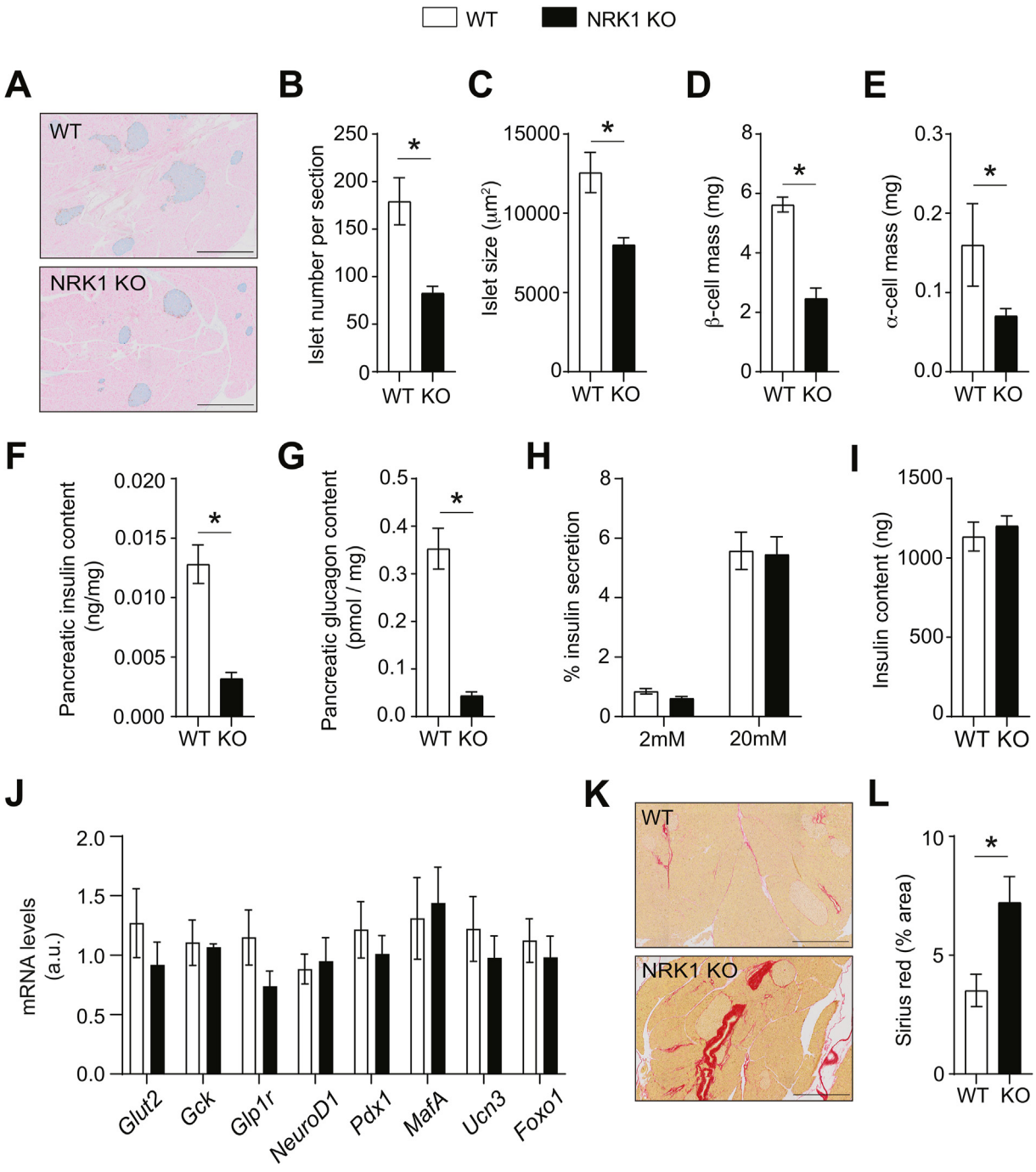

Figure 5: Pancreatic defects in aged NRK1 KO mice. (A—E) Pancreas from 24 month old wild type (WT) and NRK1 KO mice were used for histological evaluation and the quantification of islet counts (B), islet size (C) and the respective contribution of α or β-cells to overall pancreatic mass (D—E). The scale bar in (A) stands for 500 μm. **(F—G)** Total pancreas homogenates from 24 month-old WT and NRK1 KO mice were used to analyze insulin (F) and glucagon (G) content. **(H—I)-** Pancreatic islets from 24 months-old WT and NRK1 KO mice were used for glucose-stimulated insulin secretion (GSIS) assays. In (H), % of insulin secretion to the media is shown, while (I) shows total insulin content in islets. **(J)** Total RNA was extracted from pancreatic islets of 24 months-old WT and NRK1 KO mice and multiple markers were analyzed by real time quantitative PCR. **(K—L)** Representative sirius red stating of pancreas sections from aged WT and NRK1 KO mice (K) and quantification of fibrotic depots from the different samples (L). Through the figure, white bars represent WT mice, while black bars represent NRK1 KO mice. For histology image analysis, all values are expressed as mean +/− SEM of entire pancreas sections from n = 4 per genotype (B-E; L). For all other analyses, values are expressed as mean +/− SEM of n = 7 WT mice and n = 8 NRK1 KO mice (F—G) or n = 4 per genotype (H—I) or n = 6 WT mice and n = 7 NRK1 KO mice (J). * indicates $p < 0.05$ vs. the respective WT group.

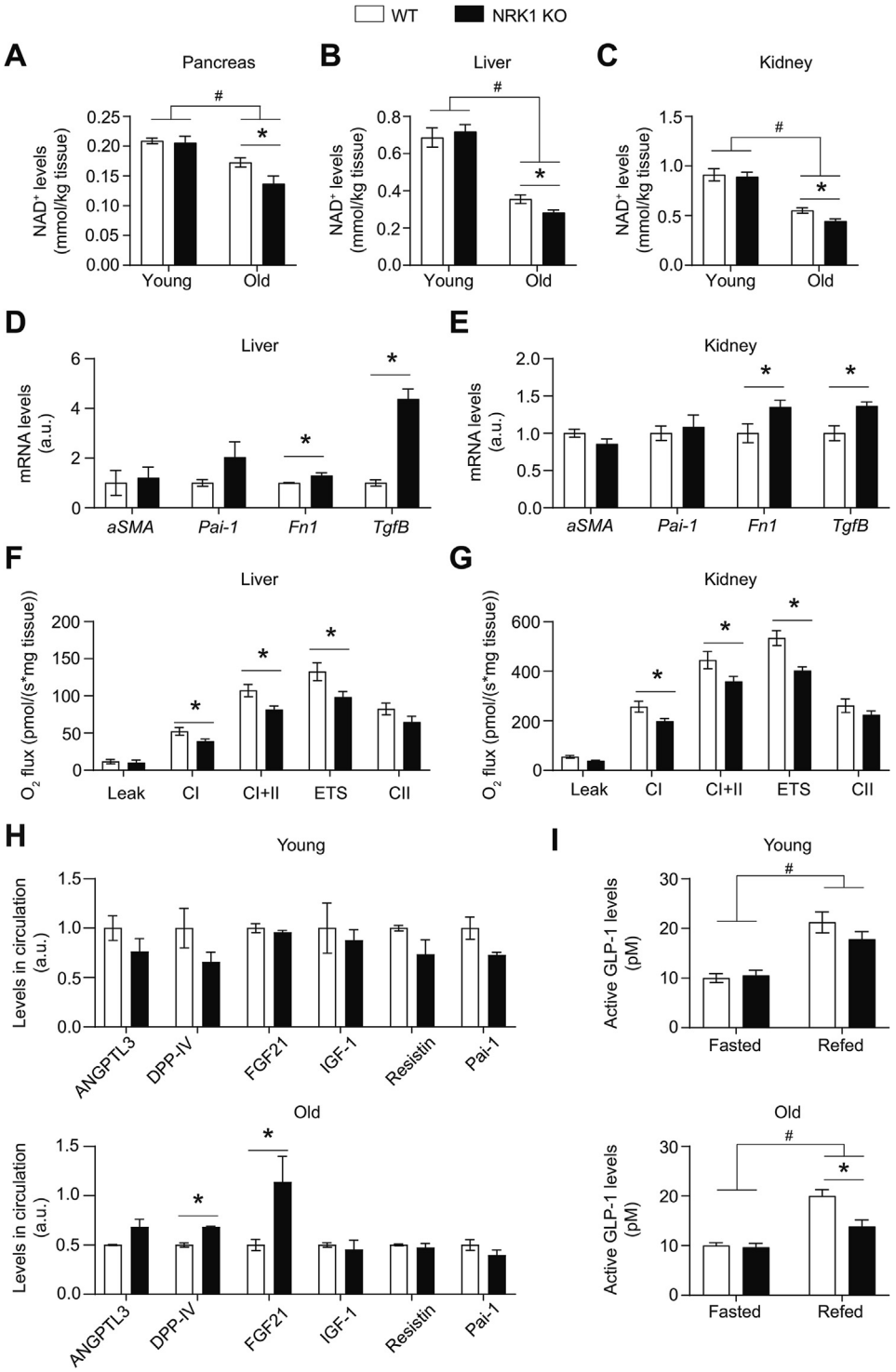

Figure 6: NRK1 deletion prompts age-related fibrosis in multiple tissues. (A–C) Pancreas, liver and kidney from 3 months-old (Young) and 24 months-old (Old) wild type (WT) or NRK1 KO mice were used to analyzed total NAD^+ content. **(D–E)** Total mRNA was extracted from liver (D) or kidney (E) from 24 month-old WT and NRK1 KO mice and fibrosis markers were evaluated by real time quantitative PCR. **(F–G)** Liver (F) and kidney (G) homogenates from 24 month old WT or NRK1 KO mice were used for high-resolution respirometry studies. Samples were treated with malate, pyruvate and glutamate to stimulate complex I in the absence of ADP (Leak), then ADP was added to evaluate coupled CI activity (CI). Next, succinate was added to stimulate Complex II and evaluate CI + CII driven respiration (CI + CII). FCCP was added to evaluate maximal electron transport system capacity (ETS). Rotenone was used then to evaluate the contribution of CII to ETS (ETC CII). **(H)** The levels of different circulating factors were evaluated in plasma from young (3 month-old) or old (24 month-old) WT and NRK1 KO mice by dot-blot analyses. **(I)** The levels of active GLP-1 in plasma were measured in young (3 month old) and old (24 month old) WT and NRK1 KO mice after a 16 h fast and 45 min after refeeding, using a commercial immunoassay (Meso Scale Discovery). Through the figure, white bars represent WT mice, while black bars represent NRK1 KO mice. All values are expressed as mean +/− SEM of n = 12 WT mice and n = 11 NRK1 KO mice (A–C), or n = 8 per genotype (D–G) or n = 4 mice per genotype (H) or n = 6 mice per genotype (I). * indicates $p < 0.05$ vs. the respective WT group.

deletion did not alter NAD^+ content in liver, kidney or pancreas in young mice (Figure 6A—C). Tissues from aged WT mice showed lower NAD^+ content, and this age-related decline in NAD^+ levels was further exacerbated in NRK1 KO mice. Specifically, NAD^+ content in pancreas, liver, and kidney was reduced by 18%, 45% and 40% in aged WT mice respectively, whereas NAD^+ declines were 33%, 60%, and 50% in NRK1 KO mice respectively.

In line with the finding that the pancreas of aged NRK1 KO mice displayed larger fibrotic areas, mRNA analyses revealed an increase in fibrosis markers, such as fibronectin 1 (*Fn1*) or the transforming growth factor B (*TgfB*), in liver and kidney (Figure 6D—E). We also analyzed mitochondrial respiratory capacity in tissues from aged WT and NRK1 KO mice. The results revealed that NRK1 deficiency led to impaired respiratory capacity in the liver and kidney when stimulating Complex I (CI), Complex I + II (CII) or maximal electron transport capacity (ETS) (Figure 6F—G). No differences were observed in maximal CII activity (ETS CII) (Figure 6F—G), suggesting that the respiratory deficits stem from Complex I. However, the impaired respiratory capacity in aged NRK1 KO mice was tissue specific, as no alterations were observed in muscle (Figure S6A). Altogether, these results suggest that, upon aging, whole-body NRK1 deficiency leads to compromised NAD^+ levels, impaired mitochondrial respiratory capacity and increased fibrotic depositions in multiple tissues.

The defects observed in liver and kidney from aged NRK1 KO mice led us to hypothesize that dysfunctional elements in these, and possibly other, tissues could influence pancreatic β-cell by altering the levels of circulating hormones or peptides. Young NRK1 KO mice did not show significant alterations in the circulating levels of any of the panel of hormones/peptides tested (Figure 6H). However, some profound changes were observed upon aging. Notably, the levels of the Dipeptidyl peptidase-IV (DPP-IV) and the fibroblast growth factor 21 (FGF21) were elevated in aged NRK1 KO mice (Figure 6H). Interestingly, circulating DPP-IV levels were also significantly higher in HFD-fed NRK1 KO mice (Figure S6B), indicating that increased DPP-IV in plasma is a common feature of NRK1 KO mice upon lifestyle challenges. In contrast, no changes in DPP-IV were observed in NRK1 BKO mice on a HFD (Fig.S6C), further supporting that the changes in circulating factors do not stem from a deficiency of NRK1 in β-cells. Lastly, we hypothesized that the alterations in DPP-IV could impact the circulating levels of GLP-1. To evaluate this point, active GLP-1 levels were measured in plasma samples from young and old WT and NRK1 KO mice that were overnight fasted and then refed for 45 min. In the fasted state, GLP-1 levels were comparable between WT and NRK1 KO mice irrespectively of their age (Figure 6I). Upon refeeding, GLP-1 similarly increased in young WT and NRK1 KO mice (Figure 6I). However, aged NRK1 KO mice showed significantly lower GLP-1 levels when refed, compared to their WT littermates (Figure 6I). Collectively, our data suggests the alteration of systemic factors in NRK1 KO mice could lead to defective pancreatic β-cell function.

4. DISCUSSION

The fact that eukaryotes have exquisitely conserved multiple independent paths to generate NAD^+ suggests that the different NAD^+ precursors could have some functional uniqueness. Work with genetic loss-of-function models has highlighted how NAM is the most widely used precursor to sustain tissue NAD^+ levels in mammals. The deletion of NAMPT in mouse skeletal muscle led to a dramatic ~90% decrease in NAD^+ content [38,39], while the deletion in liver promoted a ~50% reduction in hepatic NAD^+ levels [40]. In contrast, the genetic ablation of the nicotinic acid phophoribosyltransferase (NAPRT) or NAD synthase (NADSYN) did not alter hepatic NAD^+ levels [41], suggesting that NA is not essential to sustain hepatic NAD^+ in mice. Similarly, our current and previous results indicate that NRK1 deficiency does not alter tissue NAD^+ content in young healthy mice [25,28]. However, we report here that NRK1 deficiency leads to defefective NAD^+ levels in liver, kidney and pancreas in aged mice. This goes in line with our previous observations indicating that, upon high-fat feeding, NRK1 deficient livers showed lower NAD^+ levels than those of control littermates [28]. Given that NRK1 knockout mice can synthesize NAD^+ from NA and NAM [25], our data suggest that NR metabolism could be required to sustain NAD^+ levels upon physiological challenges. Of note, NRK1 also mediates NAD^+ synthesis from nicotinic acid riboside (NAR) [42]. Hence, in addition to NR, deficient NAR metabolism could also contribute to the phenotypes of the NRK1 KO mice.

This work describes the role of NRK1 and NR metabolism in the pancreas. Our results demonstrate that NRK1 is weakly detected in total pancreas homogenates. This is in great part due to the near absent expression of NRK1 in exocrine cells, which represent the major cell type in the pancreas [43]. In contrast, NRK1 is more abundant in pancreatic islets. Furthermore, the fact that *Nmrk1* mRNA is barely detected in islets from NRK1 BKO mice suggests that β-cells are the cell type accounting for NRK1 expression in the islet. However, given that β-cells are also the most predominant cell type in mouse islets [43], expression in other islet cell type (e.g. α-cells) cannot be fully ruled out. Our work on isolated islets demonstrates that NRK1 is necessary for NR to increase NAD^+ levels. Some mammalian cells also synthesize NAD^+ from NR by cleaving NR at the N—glycosidic bond, releasing NAM, which can then be used to generate NAD^+ via the NAMPT path [44]. Our results suggest that this second route plays a rather minor role in pancreatic islets, as NRK1 deletion fully blunted the effect of NR on NAD^+ levels. Interestingly, the treatment of isolated islets with NR did not alter GSIS, suggesting that increasing NAD^+ levels in the pancreatic islets from young, healthy micedoes not influence GSIS. The study of the impact of NAD^+ precursors on GSIS has provided disparate observations in the literature. Old studies using perifusion of isolated rat pancreatic islets indicated that NAM could increase GSIS [45]. Importantly, this required NAM concentrations of 5 mM or higher, which are far above physiological ranges [12]. In contrast, NA treatment has been reported to impair GSIS [46,47]. However, this action of NA might be not be related to its role as a NAD^+ precursor, but to the activation of GPR109A [46,47]. The works using NMN have also rendered mixed results, with one study reporting that acute NMN treatment increased GSIS in isolated mouse islets [9], while another did not see such effects upon chronic administration of NMN using human islets [8]. Where most studies converge, however, is that NMN can improve GSIS in pancreatic islets when insulin secretion is compromised by inflammatory cytokines and lipotoxicity or when NAD^+ content is decreased [8—10]. This suggests that the benefits of NAD^+ boosting molecules on GSIS might require a situation of cellular stress and damage. While the existence of a NMN transporter has been proposed [48], most works to date suggest that NMN requires dephosphorylation to NR in order to enter cells through equilibrative nucleoside transporters [24,25,49]. Therefore, NMN and NR treatments should render very similar outcomes on pancreatic islet function.

The concept that NAD^+ deficits could sensitize mice to the development of metabolic complications has been shown in tissue-specific NAMPT knockout models [50] and in NAMPT heterozygous mice [10]. In line with this, previous findings in our lab indicated that the specific deletion of NRK1 in the liver exacerbated diet-induced hepatic

damage [28]. Here, using a whole body NRK1 KO model, we demonstrate that absence of NRK1 sensitizes mice to diet or age-induced impairments in glucose control and pancreatic β-cell function. Glucose intolerance in NRK1 KO mice on HFD was accompanied by compromised GSIS from pancreatic β-cells. Notably, this led to hypertrophic pancreatic islets to compensate for the dysfunction in GSIS. In addition, NRK1 KO mice displayed several alterations in islet gene expression in situations of HFD, including a dramatic decrease in *MafA* expression. MafA is a transcription factor that is critical for insulin expression in pancreatic β cells [51]. In line with this, insulin content was downregulated in islets from obese NRK1 KO mice, even if we did not see changes in *Ins1* or *Ins2* mRNA levels (data not shown). The downregulation of *MafA* expression provides a very plausible mechanistic link to the phenotype NRK1 KO mice on a HFD, as *MafA* is also downregulated in islets from type 2 diabetic rodents and humans [52] and the genetic deletion of *MafA* in mice is enough to prompt glucose intolerance due to impaired insulin secretion [53]. We also observed a clear tendency for a decrease in the expression of the glucokinase gene (*Gck*), which might further contribute to altered glucose metabolism in HFD-fed NRK1 KO mice by compromising β-cell's ability to secrete insulin. In contrast, the pathological profile of aged NRK1 KO islets did not seem to be linked to decreased expresson of *MafA* or *Gck*. Accordingly, isolated islets from old NRK1 KO mice displayed comparable insulin content and GSIS capacity to that of age-matched WT mice. Instead, the pancreatic tissue of aged NRK1 KO mice was characterized by lower islet counts, reduced islet size and exacerbated fibrosis, ultimately leading to a failure in secreting sufficient insulin upon glucose challenges. The development of age-related pancreatic fibrosis is well documented in the literature [54] and is largely triggered by reactive oxygen species (ROS)- and inflammation-driven activation of pancreatic stellate cells [55]. Interestingly, fibrotic tissues display reduced NAD^+ content, and the supplementation with NAD^+ precursors has been shown to prevent the development of fibrosis in kidney and liver, irrespectively of whether it was induced by diet, pharmacological agents or genetic manipulations [56–59]. Collectively, our data indicates that the inability to use NR as a NAD^+ precursor sensitizes the pancreas for impaired GSIS, yet through different mechanism in the pathophysiological contexts of obesity and aging (Figure 7).

Another important point of our work is that the NRK1 BKO model did not recapitulate the pancreatic functional impairments of the NRK1 KO model. This suggests that the defects in pancreatic β cells could be consequent to systemic alterations emerging from other tissues. Nevertheless, some limitations of the studies in NRK1 BKO mice must be pointed out. First, we used floxed mice, instead of mice expressing the Cre recombinase (without floxed genes) as control mice. The expression of the Cre recombinase under the *Ins1* promoter did not lead to altered glucose homeostasis under normal housing conditions in previous studies [29]. This seems to be confirmed in this work, as the NRK1 BKO mice did not show any major metabolic phenotype. However, we cannot completely rule out that Cre recombinase could neutralize the effects driven by NRK1 deletion upon high-fat feeding or

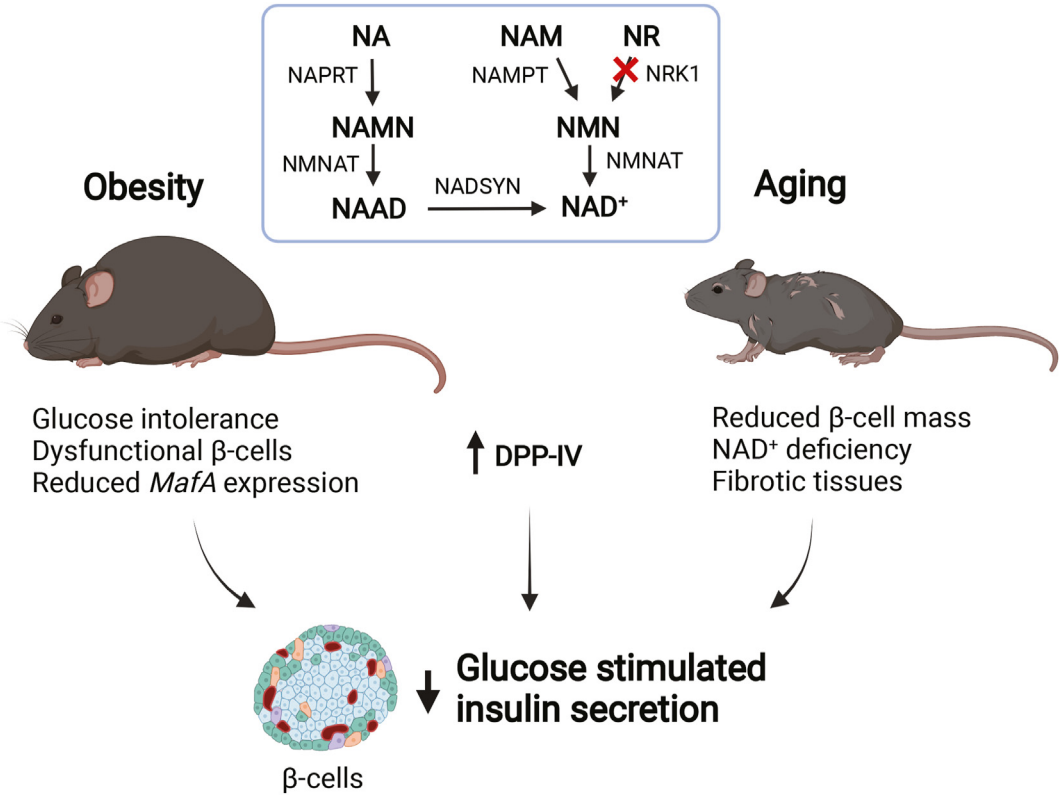

Figure 7: Summary of diet and age-related pancreatic β-cell defects in NRK1 KO mice. NRK1 KO mice cannot utilize nicotinamide riboside (NR) as a NAD^+ precursor, but can use other common NAD^+ precursors, such as nicotinamide (NAM) or nicotinic acid (NA). When submitted to a high-fat diet, NRK1 KO mice displayed exacerbated glucose intolerance and impaired glucosestimulated insulin secretion. A similar phenotype is observed in aged NRK1 KO mice. While impaired pancreatic function in obese NRK1 KO seems to stem from dysfunctional β-cells and altered islet gene expression, the impairments in aging rather seem to stem from reduced β–cell mass and pancreatic fibrosis. Our research also suggests that a common factor that could contribute to impaired glucose stimulated insulin secretion in both scenarios (obesity and aging) is an increase in circulating DPP-IV levels. The figure was created with BioRender.com.

aging. A second important point to mention is that the NRK1 BKO cohorts were on a mixed Bl/6J and Bl/6NTac background, while the experiments on whole body NRK1 KO mice were on pure Bl/6NTac background. The Bl/6J line has a mutation in the nicotinamide nucleotide transhydrogenase (*Nnt*) gene, which can contribute to exacerbate diet-induced glucose intolerance [60]. Given the breeding strategies used to generate NRK1 BKO mice (see Section 2.1), the *Nnt* mutation was never present in homozygosity. Accordingly, the glucose and insulin excursions were comparable between control *Nmrk1* floxed mice and WT mice, suggesting a weak impact of the residual Bl/6J background in our studies.

Aged NRK1 KO mice displayed reduced NAD^+ levels and mitochondrial respiratory capacity in tissues such as kidney and liver. Interestingly, mitochondrial respiration was unaltered in skeletal muscle. This is in line with the fact that NRK1 expression is high in liver and kidney, but modest in muscle [25]. Also, muscle harbors NRK2 and high NAMPT content, which could allow sustaining NAD^+ levels in situations of NRK1 deficiency [27,38]. Our quest for alterations in circulating factors rendered several interesting observations. Most notably, we detected how NRK1 deletion led to increased circulating DPP-IV levels, both in the contexts of obesity and aging. DPP-IV is a serine exopeptidase that cleaves and inactivates a broad range of growth factors and hormones [61]. Most notably, it degrades the glucagon like peptide-1 (GLP-1), a hormone that acutely enhances GSIS and β-cell survival [62]. Accordingly, the postprandial increase in circulating active GLP-1 levels was compromised in aged NRK1 KO mice, but not in young mice. The increase in DPP-IV could explain why NRK1 deficiency leads to reduced circulating GLP-1 levels and ultimately pancreatic β-cell failure. However, at this stage, the data remains correlative and lower GLP-1 levels could be consequent to other factors beyond the increase in circulating DPP-IV. Interestingly, increased DPP-IV levels are observed in obese patients and correlate with a higher risk for the development of metabolic complications [63]. Moreover, increased DPP-IV could also provide a link with the fibrotic states detected in aged NRK1 KO mice, as DPP-IV can trigger multiple processes leading to fibrotic extracellular matrix depositions [64,65]. Oppositely, the inhibition of DPP-IV has been shown to attenuate fibrosis in liver [65,66] and kidney [67–69]. Therefore, high levels of DPP-IV could contribute to the enhanced liver and kidney fibrosis observed in NRK1 KO mice. In addition to DPP-IV, we also observed an increase in circulating FGF21 levels. This could be consequent to the pronounced impairment in mitochondrial respiratory capacity observed in different tissues from aged NRK1 KO mice [70–72]. Increased circulating levels of FGF21 have also been observed in human diabetic patients [73,74]. Finally, FGF21 deficiency leads to pancreatic hyperplasia [75,76], opening the possibility that the increased FGF21 levels observed in aged NRK1 KO mice might contribute to their decreased β-cell mass.

Collectively, our results illustrate that while *Nmrk1* expression levels do not change in the situation of obesity and aging (Figure S7), NRK1-dependent routes are required to sustain NAD^+ levels and functionality of multiple tissues, including pancreatic β-cells, in situations of obesity and ageing. Our data also suggests that supplementation of NR or NAR could be used to ameliorate glucose homeostasis in insulin resistant pre-diabetic patients. However, recent clinical efforts have shown that NR supplementation failed to improve glucose tolerance and pancreatic function markers in obese pre-diabetic individuals [77,78]. An important point, however, is that NR is largely degraded in the gastrointestinal tract [41] and in circulation [25], rendering NAM or NA. Hence, the effects of native NR can be curtailed by its degradation when using regular supplementation strategies. While this work identifies the uniqueness of nucleoside-based precursors and the indications where NR could provide therapeutic advantages vs. classic NAM or NA, further efforts will be needed to generate more stable forms for clinical practice.

AUTHOR CONTRIBUTIONS

AC, JR and CC designed the project. AC, JR, JLSG, EC, JGG, MVA, AS and CC performed animal phenotyping experiments. AC and JLSG performed pancreatic islet studies. MJ designed and generated all plasmids. AC and GJ performed image analyses. AC, MJ, and MR performed mRNA, protein and NAD^+ analyses. AC, SM and AZ performed transcriptomic and statistical analyses. AC and CC wrote the manuscript and all authors contributed to revision and edits.

DATA AVAILABILITY

Data will be made available on request.

ACKNOWLEDGEMENTS

The authors wish to thank Roy Combe and the entire team of the Phenotyping Unit, Center of PhenoGenomics (CPG) at EPFL, for their technical and scientific support in mouse phenotyping experiments. We thank Jessica Sordet-Dessimoz and the team at the histology facilities at EPFL for their help with processing mouse tissues for imaging. We would also like to thank Dr. Eija Heikkila for her help in setting up techniques related to the study of β-cell biology. We are also grateful to Dr. Marine Kraus and Dr. Maria Marques de Lima for guidance and advice on the implementation and interpretation of pancreatic islet work. The illustration in Figure 7 was created with BioRender.com. This research was funded by Nestlé Research Ltd. CC and MVA were also funded by the EU Marie Skłodowska-Curie ITN-ChroMe (H2020-MSCA-ITN-2015-ChroMe project number 675610).

CONFLICT OF INTEREST

All authors are or were employees of Nestlé Research Ltd., Société des Produits Nestlé SA., while performing this research.

APPENDIX A. SUPPLEMENTARY DATA

Supplementary data to this article can be found online at https://doi.org/10.1016/j.molmet.2022.101605.

REFERENCES

[1] Leibson, C.L., Williamson, D.F., Melton 3rd, L.J., Palumbo, P.J., Smith, S.A., Ransom, J.E., et al., 2001. Temporal trends in BMI among adults with diabetes. Diabetes Care 24(9):1584–1589.

[2] Scheen, A.J., 2005. Diabetes mellitus in the elderly: insulin resistance and/or impaired insulin secretion? Diabetes & Metabolism(2), 31 Spec 5S27-S34.

[3] Hawley, J.A., 2004. Exercise as a therapeutic intervention for the prevention and treatment of insulin resistance. Disbetes Metabolism Research Review 20(5):383–393.

[4] Canto, C., Houtkooper, R.H., Pirinen, E., Youn, D.Y., Oosterveer, M.H., Cen, Y., et al., 2012. The NAD(+) precursor nicotinamide riboside enhances oxidative metabolism and protects against high-fat diet-induced obesity. Cell Metabolism 15(6):838–847.

[5] Yoshino, J., Mills, K.F., Yoon, M.J., Imai, S., 2011. Nicotinamide mononucleotide, a key NAD(+) intermediate, treats the pathophysiology of diet- and age-induced diabetes in mice. Cell Metabolism 14(4):528–536.

[6] Trammell, S.A., Weidemann, B.J., Chadda, A., Yorek, M.S., Holmes, A., Coppey, L.J., et al., 2016. Nicotinamide riboside opposes type 2 diabetes and neuropathy in mice. Scientific Reports 6:26933.

[7] Gariani, K., Menzies, K.J., Ryu, D., Wegner, C.J., Wang, X., Ropelle, E.R., et al., 2016. Eliciting the mitochondrial unfolded protein response by nicotinamide adenine dinucleotide repletion reverses fatty liver disease in mice. Hepatology 63(4):1190–1204.

[8] Spinnler, R., Gorski, T., Stolz, K., Schuster, S., Garten, A., Beck-Sickinger, A.G., et al., 2013. The adipocytokine Nampt and its product NMN have no effect on beta-cell survival but potentiate glucose stimulated insulin secretion. PLoS One 8(1):e54106.

[9] Caton, P.W., Kieswich, J., Yaqoob, M.M., Holness, M.J., Sugden, M.C., 2011. Nicotinamide mononucleotide protects against pro-inflammatory cytokine-mediated impairment of mouse islet function. Diabetologia 54(12):3083–3092.

[10] Revollo, J.R., Körner, A., Mills, K.F., Satoh, A., Wang, T., Garten, A., et al., 2007. Nampt/PBEF/Visfatin regulates insulin secretion in beta cells as a systemic NAD biosynthetic enzyme. Cell Metabolism 6(5):363–375.

[11] Covarrubias, A.J., Perrone, R., Grozio, A., Verdin, E., 2021. NAD(+) metabolism and its roles in cellular processes during ageing. Nature Reviews Molecular Cell Biology 22(2):119–141.

[12] Canto, C., Menzies, K.J., Auwerx, J., 2015. NAD(+) metabolism and the control of energy homeostasis: a balancing act between mitochondria and the nucleus. Cell Metabolism 22(1):31–53.

[13] Boutant, M., Joffraud, M., Kulkarni, S.S., Garcia-Casarrubios, E., Garcia-Roves, P.M., Ratajczak, J., et al., 2015. SIRT1 enhances glucose tolerance by potentiating brown adipose tissue function. Molecular Metabolism 4(2):118–131.

[14] Pfluger, P.T., Herranz, D., Velasco-Miguel, S., Serrano, M., Tschöp, M.H., 2008. Sirt1 protects against high-fat diet-induced metabolic damage. Proceedings of the National Academy of Sciences of the U S A 105(28):9793–9798.

[15] Banks, A.S., Kon, N., Knight, C., Matsumoto, M., Gutiérrez-Juarez, R., Rossetti, L., et al., 2008. SirT1 gain of function increases energy efficiency and prevents diabetes in mice. Cell Metabolism 8(4):333–341.

[16] Herranz, D., Muñoz-Martin, M., Cañamero, M., Mulero, F., Martinez-Pastor, B., Fernandez-Capetillo, O., et al., 2010. Sirt1 improves healthy ageing and protects from metabolic syndrome-associated cancer. Nature Communications 1:3.

[17] Moynihan, K.A., Grimm, A.A., Plueger, M.M., Bernal-Mizrachi, E., Ford, E., Cras-Méneur, C., et al., 2005. Increased dosage of mammalian Sir2 in pancreatic beta cells enhances glucose-stimulated insulin secretion in mice. Cell Metabolism 2(2):105–117.

[18] Luu, L., Dai, F.F., Prentice, K.J., Huang, X., Hardy, A.B., Hansen, J.B., et al., 2013. The loss of Sirt1 in mouse pancreatic beta cells impairs insulin secretion by disrupting glucose sensing. Diabetologia 56(9):2010–2020.

[19] Bordone, L., Motta, M.C., Picard, F., Robinson, A., Jhala, U.S., Apfeld, J., et al., 2006. Sirt1 regulates insulin secretion by repressing UCP2 in pancreatic beta cells. PLoS Biology 4(2):e31.

[20] Pinho, A.V., Bensellam, M., Wauters, E., Rees, M., Giry-Laterriere, M., Mawson, A., et al., 2015. Pancreas-specific sirt1-deficiency in mice compromises beta-cell function without development of hyperglycemia. PLoS One 10(6):e0128012.

[21] Lee, J.H., Song, M.Y., Song, E.K., Kim, E.K., Moon, W.S., Han, M.K., et al., 2009. Overexpression of SIRT1 protects pancreatic beta-cells against cytokine toxicity by suppressing the nuclear factor-kappaB signaling pathway. Diabetes 58(2):344–351.

[22] Kitamura, Y.I., Kitamura, T., Kruse, J.P., Raum, J.C., Stein, R., Gu, W., et al., 2005. FoxO1 protects against pancreatic beta cell failure through NeuroD and MafA induction. Cell Metabolism 2(3):153–163.

[23] Benyo, Z., Gille, A., Kero, J., Csiky, M., Suchankova, M.C., Nüsing, R.M., et al., 2005. GPR109A (PUMA-G/HM74A) mediates nicotinic acid-induced flushing. Journal of Clinical Investigation 115(12):3634–3640.

[24] Nikiforov, A., Dölle, C., Niere, M., Ziegler, M., 2011. Pathways and subcellular compartmentation of NAD biosynthesis in human cells: from entry of extracellular precursors to mitochondrial NAD generation. Journal of Biological Chemistry 286(24):21767–21778.

[25] Ratajczak, J., Joffraud, M., Trammell, S.A., Ras, R., Canela, N., Boutant, M., et al., 2016. NRK1 controls nicotinamide mononucleotide and nicotinamide riboside metabolism in mammalian cells. Nature Communications 7:13103.

[26] Bieganowski, P., Brenner, C., 2004. Discoveries of nicotinamide riboside as a nutrient and conserved NRK genes establish a Preiss-Handler independent route to NAD+ in fungi and humans. Cell 117(4):495–502.

[27] Fletcher, R.S., Ratajczak, J., Doig, C.L., Oakey, L.A., Callingham, R., Da Silva Xavier, G., et al., 2017. Nicotinamide riboside kinases display redundancy in mediating nicotinamide mononucleotide and nicotinamide riboside metabolism in skeletal muscle cells. Molecular Metabolism 6(8):819–832.

[28] Sambeat, A., Ratajczak, J., Joffraud, M., Sanchez-Garcia, J.L., Giner, M.P., Valsesia, A., et al., 2019. Endogenous nicotinamide riboside metabolism protects against diet-induced liver damage. Nature Communications 10(1):4291.

[29] Thorens, B., Tarussio, D., Maestro, M.A., Rovira, M., Heikkilä, E., Ferrer, J., 2015. Ins1(Cre) knock-in mice for beta cell-specific gene recombination. Diabetologia 58(3):558–565.

[30] Pettersson, U.S., Waldén, T.B., Carlsson, P.O., Jansson, L., Phillipson, M., 2012. Female mice are protected against high-fat diet induced metabolic syndrome and increase the regulatory T cell population in adipose tissue. PLoS One 7(9):e46057.

[31] Riant, E., Waget, A., Cogo, H., Arnal, J.F., Burcelin, R., Gourdy, P., 2009. Estrogens protect against high-fat diet-induced insulin resistance and glucose intolerance in mice. Endocrinology 150(5):2109–2117.

[32] de Souza, G.O., Wasinski, F., Donato Jr., J., 2022. Characterization of the metabolic differences between male and female C57BL/6 mice. Life Sciences 301:120636.

[33] Casimiro, I., Stull, N.D., Tersey, S.A., Mirmira, R.G., 2021. Phenotypic sexual dimorphism in response to dietary fat manipulation in C57BL/6J mice. Journal of Diabetic Complications 35(2):107795.

[34] Li, D.S., Yuan, Y.H., Tu, H.J., Liang, Q.L., Dai, L.J., 2009. A protocol for islet isolation from mouse pancreas. Nature Protocols 4(11):1649–1652.

[35] Merglen, A., Theander, S., Rubi, B., Chaffard, G., Wollheim, C.B., Maechler, P., 2004. Glucose sensitivity and metabolism-secretion coupling studied during two-year continuous culture in INS-1E insulinoma cells. Endocrinology 145(2):667–678.

[36] Canto, C., Garcia-Roves, P.M., 2015. High-resolution respirometry for mitochondrial characterization of ex vivo mouse tissues. Current Protocols in Molecular Biology 5(2):135–153.

[37] Bankhead, P., Loughrey, M.B., Fernandez, J.A., Dombrowski, Y., McArt, D.G., Dunne, P.D., et al., 2017. QuPath: open source software for digital pathology image analysis. Scientific Reports 7(1):16878.

[38] Frederick, D.W., Loro, E., Liu, L., Davila Jr, A., Chellappa, K., Silverman, I.M., et al., 2016. Loss of NAD homeostasis leads to progressive and reversible degeneration of skeletal muscle. Cell Metabolism 24(2):269–282.

[39] Basse, A.L., Angerholm, M., Farup, J., Dalbram, E., Nielsen, J., Ørtenblad, N., et al., 2021. Nampt controls skeletal muscle development by maintaining Ca(2+) homeostasis and mitochondrial integrity. Molecular Metabolism 53:101271.

[40] Dall, M., Trammell, S.A., Asping, M., Hassing, A.S., Agerholm, M., Vienberg, S.G., et al., 2019. Mitochondrial function in liver cells is resistant to perturbations in NAD(+) salvage capacity. Journal of Biological Chemistry 294(36):13304–13326.

[41] Yaku, K., Palikhe, S., Izumi, H., Yoshida, T., Hikosaka, K., Hayat, F., et al., 2021. BST1 regulates nicotinamide riboside metabolism via its glycohydrolase and base-exchange activities. Nature Communications 12(1):6767.

[42] Tempel, W., Rabeh, W.M., Bogan, K.L., Belenky, P., Wojcik, M., Seidle, H.F., et al., 2007. Nicotinamide riboside kinase structures reveal new pathways to NAD+. PLoS Biology 5(10):e263.
[43] Tsuchitani, M., Sato, J., Kokoshima, H., 2016. A comparison of the anatomical structure of the pancreas in experimental animals. Journal of Toxicologic Pathology 29(3):147–154.
[44] Kulikova, V., Shabalin, K., Nerinovski, K., Yakimov, A., Svetlova, M., Solovjeva, L., et al., 2019. Degradation of extracellular NAD(+) intermediates in cultures of human HEK293 cells. Metabolites 9(12).
[45] Zawalich, W.S., Dye, E.S., Matschinsky, F.M., 1979. Nicotinamide modulation of rat pancreatic islet cell responsiveness in vitro. Hormone and Metabolic Research 11(8):469–471.
[46] Li, H.M., Zhang, M., Xu, S.T., Li, D.Z., Zhu, L.Y., Peng, S.W., et al., 2011. Nicotinic acid inhibits glucose-stimulated insulin secretion via the G protein-coupled receptor PUMA-G in murine islet beta cells. Pancreas 40(4):615–621.
[47] Chen, L., So, W.Y., Li, S.Y., Cheng, Q., Boucher, B.J., Leung, P.S., 2015. Niacin-induced hyperglycemia is partially mediated via niacin receptor GPR109a in pancreatic islets. Molecular and Cellular Endocrinology 404:56–66.
[48] Grozio, A., Mills, K.F., Yoshino, J., Bruzzone, S., Sociali, G., Tokizane, K., et al., 2019. Slc12a8 is a nicotinamide mononucleotide transporter. Nature Metabolism 1(1):47–57.
[49] Grozio, A., Sociali, G., Sturla, L., Caffa, I., Soncini, D., Salis, A., et al., 2013. CD73 protein as a source of extracellular precursors for sustained NAD+ biosynthesis in FK866-treated tumor cells. Journal of Biological Chemistry 288(36):25938–25949.
[50] Dall, M., Hassing, A.S., Niu, L., Nielsen, T.S., Ingerslev, L.R., Sulek, K., et al., 2021. Hepatocyte-specific perturbation of NAD(+) biosynthetic pathways in mice induces reversible nonalcoholic steatohepatitis-like phenotypes. Journal of Biological Chemistry 297(6):101388.
[51] Kataoka, K., Han, S.I., Shioda, S., Hirai, M., Nishizawa, M., Handa, H., 2002. MafA is a glucose-regulated and pancreatic beta-cell-specific transcriptional activator for the insulin gene. Journal of Biological Chemistry 277(51):49903–49910.
[52] Guo, S., Dai, C., Guo, M., Taylor, B., Harmon, J.S., Sander, M., et al., 2013. Inactivation of specific beta cell transcription factors in type 2 diabetes. Journal of Clinical Investigation 123(8):3305–3316.
[53] Zhang, C., Moriguchi, T., Kajihara, M., Esaki, R., Harada, A., Shimohata, H., et al., 2005. MafA is a key regulator of glucose-stimulated insulin secretion. Molecular and Cellular Biology 25(12):4969–4976.
[54] Lohr, J.M., Panic, N., Vujasinovic, M., Verbeke, C.S., 2018. The ageing pancreas: a systematic review of the evidence and analysis of the consequences. Journal of Internal Medicine 283(5):446–460.
[55] Huang, C., Iovanna, J., Santofimia-Castano, P., 2021. Targeting fibrosis: the bridge that connects pancreatitis and pancreatic cancer. International Journal of Molecular Sciences 22(9).
[56] Giroud-Gerbetant, J., Joffraud, M., Giner, M.P., Cercillieux, A., Bartova, S., Makarov, M.V., et al., 2019. A reduced form of nicotinamide riboside defines a new path for NAD(+) biosynthesis and acts as an orally bioavailable NAD(+) precursor. Molecular Metabolism 30:192–202.
[57] Jia, Y., Kang, X., Tan, L., Ren, Y., Qu, L., Tang, J., et al., 2021. Nicotinamide mononucleotide attenuates renal interstitial fibrosis after AKI by suppressing tubular DNA damage and senescence. Frontiers in Physiology 12:649547.
[58] Pham, T.X., Bae, M., Kim, M.B., Lee, Y., Hu, S., Kang, H., et al., 2019. Nicotinamide riboside, an NAD+ precursor, attenuates the development of liver fibrosis in a diet-induced mouse model of liver fibrosis. Biochimica et Biophysica Acta, Molecular Basis of Disease 1865(9):2451–2463.
[59] Shi, B., Wang, W., Korman, B., Kai, L., Wang, Q., Wei, J., et al., 2021. Targeting CD38-dependent NAD(+) metabolism to mitigate multiple organ fibrosis. iScience 24(1):101902.
[60] Nicholson, A., Reifsnyder, P.C., Malcolm, R.D., Lucas, C.A., MacGregor, G.R., Zhang, W., et al., 2010. Diet-induced obesity in two C57BL/6 substrains with intact or mutant nicotinamide nucleotide transhydrogenase (Nnt) gene. Obesity 18(10):1902–1905.
[61] Rohrborn, D., Wronkowitz, N., Eckel, J., 2015. DPP4 in diabetes. Frontiers in Immunology 6:386.
[62] Gilbert, M.P., Pratley, R.E., 2020. GLP-1 analogs and DPP-4 inhibitors in type 2 diabetes therapy: review of head-to-head clinical trials. Frontiers in Endocrinology 11:178.
[63] Sell, H., Blüher, M., Klöting, N., Schlich, R., Willems, M., Ruppe, F., et al., 2013. Adipose dipeptidyl peptidase-4 and obesity: correlation with insulin resistance and depot-specific release from adipose tissue in vivo and in vitro. Diabetes Care 36(12):4083–4090.
[64] Zhang, K.W., Liu, S.Y., Jia, Y., Zou, M.L., Teng, Y.Y., Chen, Z.H., et al., 2022. Insight into the role of DPP-4 in fibrotic wound healing. Biomedicine & Pharmacotherapy 151:113143.
[65] Lay, A.J., Zhang, H.E., McCaughan, G.W., Gorrell, M.D., 2019. Fibroblast activation protein in liver fibrosis. Frontiers in Bioscience 24(1):1–17.
[66] Kawakubo, M., Tanaka, M., Ochi, K., Watanabe, A., Saka-Tanaka, M., Kanamori, Y., et al., 2020. Dipeptidyl peptidase-4 inhibition prevents nonalcoholic steatohepatitis-associated liver fibrosis and tumor development in mice independently of its anti-diabetic effects. Scientific Reports 10(1):983.
[67] Shi, S., Koya, D., Kanasaki, K., 2016. Dipeptidyl peptidase-4 and kidney fibrosis in diabetes. Fibrogenesis & Tissue Repair 9:1.
[68] Tsuprykov, O., Ando, R., Reichetzeder, C., von Websky, K., Antonenko, V., Sharkovska, Y., et al., 2016. The dipeptidyl peptidase inhibitor linagliptin and the angiotensin II receptor blocker telmisartan show renal benefit by different pathways in rats with 5/6 nephrectomy. Kidney International 89(5):1049–1061.
[69] Tanaka, Y., Kume, S., Chin-Kanasaki, M., Araki, H., Araki, S.I., Ugi, S., et al., 2016. Renoprotective effect of DPP-4 inhibitors against free fatty acid-bound albumin-induced renal proximal tubular cell injury. Biochemical and Biophysical Research Communications 470(3):539–545.
[70] Kim, K.H., Jeong, Y.T., Oh, H., Kim, S.H., Cho, J.M., Kim, Y.N., et al., 2013. Autophagy deficiency leads to protection from obesity and insulin resistance by inducing Fgf21 as a mitokine. Nature Medicine 19(1):83–92.
[71] Lehtonen, J.M., Auranen, M., Darin, N., Sofou, K., Bindoff, L., Hikmat, O., et al., 2016. FGF21 is a biomarker for mitochondrial translation and mtDNA maintenance disorders. Neurology 87(22):2290–2299.
[72] Davis, R.L., Liang, C., Edema-Hildebrand, F., Riley, C., Needham, M., Sue, C.M., 2013. Fibroblast growth factor 21 is a sensitive biomarker of mitochondrial disease. Neurology 81(21):1819–1826.
[73] Mraz, M., Bartlova, M., Lacinova, Z., Michalsky, M., Kasalicky, M., Haluzikova, D., et al., 2009. Serum concentrations and tissue expression of a novel endocrine regulator fibroblast growth factor-21 in patients with type 2 diabetes and obesity. Clinical Endocrinology 71(3):369–375.
[74] Cheng, X., Zhu, B., Jiang, F., Fan, H., 2011. Serum FGF-21 levels in type 2 diabetic patients. Endocrine Research 36(4):142–148.
[75] So, W.Y., Cheng, Q., Xu, A., Lam, K.S., Leung, P.S., 2015. Loss of fibroblast growth factor 21 action induces insulin resistance, pancreatic islet hyperplasia and dysfunction in mice. Cell Death & Disease 6:e1707.
[76] Singhal, G., Fisher, F.M., Chee, M.J., Tan, T.G., El Ouaamari, A., Adams, A.C., et al., 2016. Fibroblast growth factor 21 (FGF21) protects against high fat diet induced inflammation and islet hyperplasia in pancreas. PLoS One 11(2):e0148252.
[77] Dollerup, O.L., Christensen, B., Svart, M., Schmidt, M.S., Sulek, K., Ringgaard, S., et al., 2018. A randomized placebo-controlled clinical trial of nicotinamide riboside in obese men: safety, insulin-sensitivity, and lipid-mobilizing effects. The American Journal of Clinical Nutrition 108(2):343–353.
[78] Dollerup, O.L., Trammell, S.A.J., Hartmann, B., Holst, J.J., Christensen, B., Møller, N., et al., 2019. Effects of nicotinamide riboside on endocrine pancreatic function and incretin hormones in nondiabetic men with obesity. Journal of Clinical Endocrinology and Metabolism 104(11):5703–5714.

